E-20-G57
#1

Draft

Final Report

October 2001

Dynamic Thermal and Chemical Behavior of Membrane Interface Probe

Contract Number: GA0073
Education, Research and Development Agency (ERDA)
WSRC Task Order Agreement: KG18086-O

Principal Investigator:
Kurt D. Pennell, Ph.D.
Associate Professor
School of Civil & Environmental Engineering
Georgia Institute of Technology
200 Bobby Dodd Way
Atlanta, GA 30332-0512
Tel: 404-894-9365
Fax: 404-385-0776
e-mail: kpennell@ce.gatech.edu

Project Coordinator:
Jed Costanza

Period of Performance:
21 March 2001 to 30 September 2001

Report Date:
15 October 2001

Table of Contents

List of Figures

List of Tables

Dynamic Thermal and Chemical Behavior of the Membrane Interface Probe
***Draft* Final Report: October 2001**

Contract Number: GA0073 (ERDA)
WSRC Task Order Agreement: KG18086-O
Principal Investigator: Kurt D. Pennell, Ph.D.
Project Coordinator: Jed Costanza

1.0 Project Abstract

The Membrane Interface Probe (MIP) was developed by Geoprobe® Systems to provide real-time, *in-situ* characterization of dissolved- and separate-phase volatile organic compounds (VOCs) in subsurface environments. The MIP is deployed using direct push techniques, such as a cone penetrometer or Geoprobe® machine. The MIP device utilizes a heated membrane, installed in the wall of a direct push probe, to collect vapor-phase VOC samples from the subsurface. The VOC sample is then transferred via inert carrier gas to the ground surface for chemical analysis. A detailed validation study of MIP performance was completed at five contaminated sites located in the United State and involved comparing independent analysis of soil samples co-located with in-situ MIP sample results (ESTCP, 2001). The validation study included several waste management units located on the Savannah River Site (SRS). Results obtained from this validation study indicate that MIP VOC analytical data were subject to systematic bias, which appeared to be dependent on the properties of the subsurface material, including particle size and moisture content (Costanza and Davis, 2000). Before the MIP can be utilize as a semi-quantitative characterization tool, performance of the membrane in subsurface systems must be understood. Therefore, this project was designed to elucidate processes governing the dynamic operation of the MIP through a combination of laboratory experiments and field tests.

Specific objectives were developed to investigate the relationship between soil properties and MIP behavior under controlled laboratory and field conditions. These objectives included measuring soil temperature profiles and VOC mass transfer for the MIP operating in differing soils with different moisture contents, and evaluating continuous and discrete depth MIP operation. Research tasks that directly corresponded to the stated objectives were developed and involved the construction, assembly, and development of procedures to achieve the goals stated in each objective. A test chamber filled with soil, water, and instrumented with thermocouples was used to determine the temperature distribution resulting from MIP operation. Water containing 50 mg/L trichloroethylene(TCE) was pumped through a 2mL chamber attached to the MIP to determine mass transferred from gas, water, and saturated soil. Field tests were performed at SRS to evaluate both continuous and depth discrete sample collection procedures, and the temperature dependence of the sample collection process.

Results of these studies show that the primary mode of VOC transfer through the membrane is by Knudsen diffusion, which is driven by the vapor pressure of VOC compounds exterior to the membrane. Heating the membrane serves to increase the vapor pressure and reduce

VOC residence time within the membrane. The theoretical temperature at which maximum VOC flux occurs is near 100°C. However, controlled laboratory and field tests yielded better recovery at operational temperatures between 40 and 80°C. At greater temperatures the "on-off" feedback control used to heat the membrane was found to cause large transient increases in VOC flux. It is recommended that the membrane be heated with a proportional power supply using a feedback temperature set-point between the limits of 40 and 80°C.

2.0 Introduction

The Membrane Interface Probe (MIP) was developed by Geoprobe® Systems to provide real-time, *in-situ* characterization of dissolved- and separate-phase volatile organic compounds (VOCs) in the subsurface environments. The MIP is typically deployed in conjunction with a direct push cone penetrometer or a percussion hammer rig such as a Geoprobe® machine. The MIP device employs a heated, semi-permeable membrane, installed in the wall of a direct push probe, to collect vapor-phase VOC samples from the subsurface. The VOC sample is then transferred via inert carrier gas to the ground surface for chemical analysis. A schematic diagram of the Membrane Interface Probe (U.S. Patent Number 5,639,956) is shown in Figure 2.1. With the exception of membrane failure, there is no need to retrieve the device between sampling events.

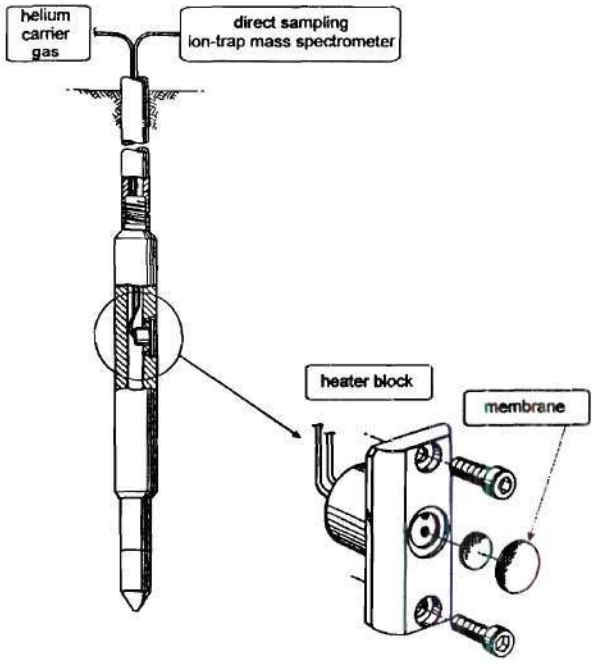

Figure 2.1 – Membrane Interface Probe

The MIP used in this project was constructed by the U.S. Army Corps of Engineers, Waterways Experiment Station, located in Vicksburg, MS. The MIP included a heater block and membrane manufactured by Geoprobe® Systems. Several modifications were made to the MIP based on prior field experiences. The most significant change was replacement of the standard Teflon™ tubing used in sample transfer to the surface with 1/8-inch ID polyether ether ketone (PEEK) tubing (3.17 mm OD x 1.57 mm ID, Alltech, Inc. part #35717). This modification significantly reduces the potential for contaminant carry-over between sample collection events.

The modified MIP also includes standard U.S. Army Corps cone penetrometer sensors. In addition, through-the-tip grouting is used to inject sealant into void space as the MIP is retracted from the subsurface. This minimizes the potential for vertical transport of chemical contamination. The cone penetrometer sensors are used for soil characterization purposes, to identify soil conditions in advance of the membrane sampling port. This allows for the

determination of the depth(s) of investigation interest while driving the MIP into the subsurface.

The membrane interface portion of the MIP consists of a circular (1.13 cm^2 area) polymer port that is permeable to gas but impermeable to most liquid phases. The permeable membrane consists of a thin (~ 0.1 cm) film of Teflon (TFE, E.I. Du Pont de Nemours & Co.) sintered onto a stainless steel screen. The membrane is imbedded into a housing that contains resistive heater coils and a thermocouple, which allows the temperature of the membrane to be maintained at approximately 120°C. VOCs migrate through the membrane into ultra-pure grade helium carrier gas that flows past the back-side of the membrane and is transferred through 31 m of tubing to the ground surface for analysis. A variety of detectors can be used to analyze the contents of the returning helium carrier gas. For this project, the detector was a direct sampling (in-line) Ion Trap Mass Spectrometer (ITMS). The direct sampling ITMS was developed by the U.S. Department of Energy, Oak Ridge National Laboratory (Wise et al., 1997).

A detailed validation study of MIP performance was completed at five contaminated sites located in the United State and involved comparing independent analysis of soil samples co-located with in-situ MIP sample results (ESTCP, 2001). The validation study included several waste management units located on the Savannah River Site (SRS). Results obtained from this validation study indicate that MIP VOC analytical data were subject to systematic bias, which appeared to be dependent on the properties of the subsurface material, including particle size and moisture content (Costanza and Davis, 2000). This report describes further testing performed in effort to minimize the observed bias, and to enhance performance of the MIP as a semi-quantitative subsurface characterization tool. This project was designed to elucidate processes governing the dynamic operation of the MIP through a combination of laboratory experiments and field tests.

The following four specific objectives were developed to systematically identify and evaluate soil properties and processes that influence performance of the MIP. Objectives 1, 2, and 3 were designed to investigate the relationship between soil properties and MIP behavior under controlled conditions, and were conducted at the laboratory scale. Objective 4 focused on field implementation of the MIP, and was intended to link information obtained from the laboratory experiments with field-scale testing.

Objective 1. Investigate the effects of soil properties on temperature profiles and resulting sample volumes collected by the MIP.

Objective 2. Evaluate the influence of soil properties on mass transfer of VOCs from contaminated soil into the MIP.

Objective 3. Assess the impact MIP operation on soil moisture profiles using MRI methods.

Objective 4. Evaluate the ability of the MIP to characterize VOCs under continuous and discrete field sampling regimes.

3.0 Experimental Methods

Four research tasks were developed that directly correspond to the research objectives stated above. Each task involved the construction and assembly of equipment and development of procedures to achieve the goals stated in each objective. The following sections provide details of experimental methods and procedures created for each task.

3.1 Task 1: Investigation of Soil Temperature Profile and MIP Sample Volume

A test chamber filled with soil, water, and instrumented with thermocouples was used to determine the temperature distribution resulting from MIP operation. The experiments were performed using two reference Ottawa Sands, Appling soil, and a clay sample provided by WSRC. Thermal influence was determined for each soil sample as a function of three water contents, air-dry, gravity drained or field capacity, and water-saturated.

3.1.1 Membrane Interface Probe

The MIP used in the laboratory experiments was constructed by the U.S. Army Corps of Engineers, Waterways Experiment Station. A standard MIP heater block and membrane was purchased from Geoprobe® Systems (U.S. Patent No. 5,639,956) and attached to a section of steel normally used for the construction of a full-scale probe. A schematic diagram of the MIP is shown in Figure 1

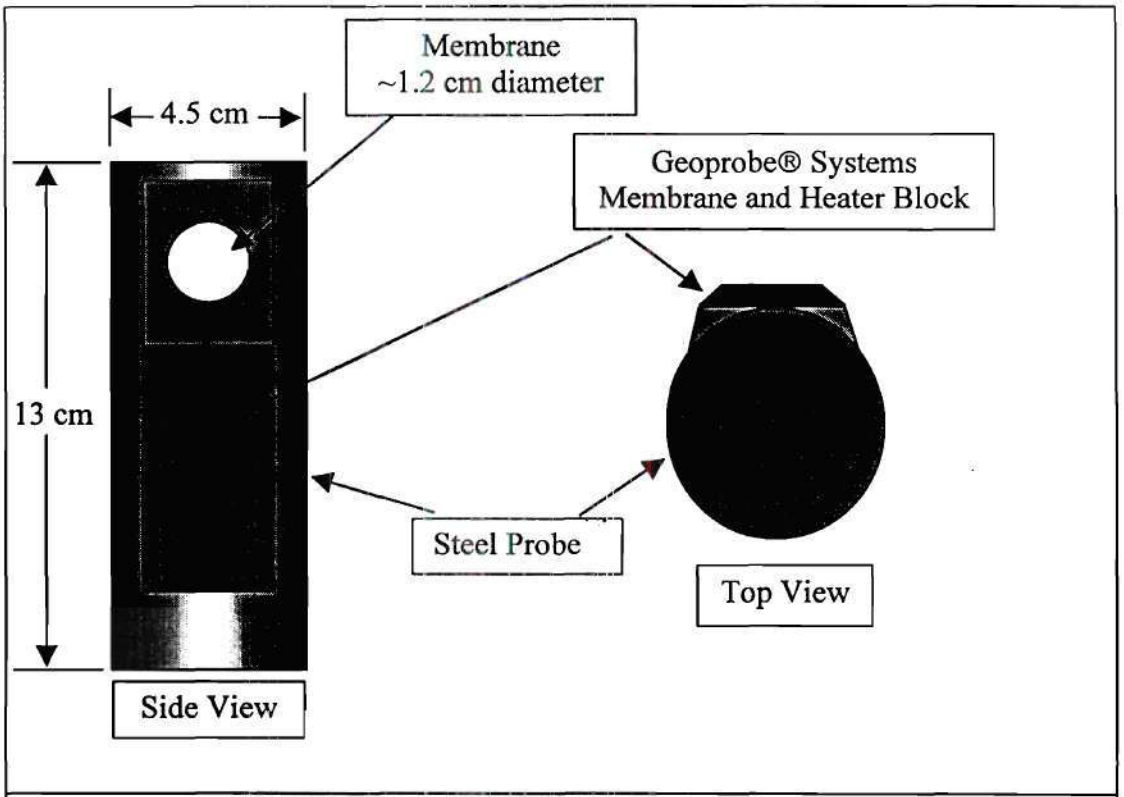

Figure 3.1 - Schematic diagram of the laboratory-scale MIP

3.1.2 Solids

Three types of unconsolidated porous media, 20-30 mesh Ottawa sand, F-70 (40-270 mesh) Ottawa sand, and Appling Soil, were selected to represent a range of soils normally encountered during operation of the MIP. The Ottawa sands were obtained from U.S. Silica (Ottawa, IL) and were used as received. Appling soil was collected from the upper 30 cm of the soil profile, corresponding to the Ap1 and Ap2 horizons, at the University of Georgia Agricultural Experiment Station, located near Eastville, GA. The soil is classified as a loamy coarse sand of the Appling series (clayey, kaolinitic thermic Typic Hapludult). Prior to use, the Appling soil was air-dried and ground to pass a 2 mm (9-mesh) sieve. Specific surface area was determined using a Micromeretics ASAP 2010 surface area analyzer, based on N_2 adsorption at 77°K, while the organic carbon content was measured using a Shimadzu TOC-5050A Total Organic Carbon (TOC) analyzer equipped with a solid sample module and a non-dispersive infrared detector. Selected properties of the three solid phases are given in Table 3.1.

Table 3.1 - Selected properties of solid phases used in laboratory experiments.

Solid Phase	Specific Surface Area (m^2/g)	Intrinsic Permeability (m^2)	Organic Carbon Content (%)
20-30 mesh Ottawa sand	0.10	3.9×10^{-10}	nd
F-70 (40-270) Ottawa sand	0.16	8.2×10^{-12}	nd
Appling Soil	3.50	1.2×10^{-11}	0.75

nd = none detected (<0.01%)

3.1.3 Test Chamber and Packing Procedure

Laboratory-scale MIP experiments were conducted within a 22.9cm diameter by 31.6cm tall Acrylic cylindrical test chamber open at the top and lined brass mesh screen along the bottom. The test chamber (Figure 3.2) was initially filled with dry sand or soil to a level 10cm from the bottom of the chamber. The MIP (shown in Figure 3.1) was then placed upright (i.e., vertical orientation) on top of the sand, and slightly offset from the center of the chamber. A second layer of soil was then added to a level even with the height of the membrane. Thermocouple leads (0.005 gauge, 91cm long, Teflon insulated, Omega Engineering Part #TC5TC-TTK36-36) were fit into a plastic holder at regular intervals and then placed in the soil to achieve known spacing from the membrane. Finally, soil was then added to a level even with the top of the chamber burying the MIP and thermocouples.

3.1.4 Temperature Measurement Procedures

A Campbell Scientific CR23X data logger was used to record the temperature at the thermocouple ends buried within the test chamber and at the thermocouple embedded within the MIP heater block. The temperatures were recorded until isothermal conditions were established. The membrane heater was then engaged for a period of 10 minutes, and the thermocouple temperatures were recorded at 0.3-second intervals for a total period of 30 minutes.

The chamber was then bottom-filled with tap water over a period of 30 minutes until standing water was observed above the upper surface of the soil. Thermocouple temperatures were again recorded until isothermal conditions were obtained. The membrane heater was then engaged for a period of 10 minutes, and thermocouple temperatures were recorded at 0.3-second intervals for a total period of 30 minutes.

The test chamber was then allowed to drain under gravity for a period of 2 hours.

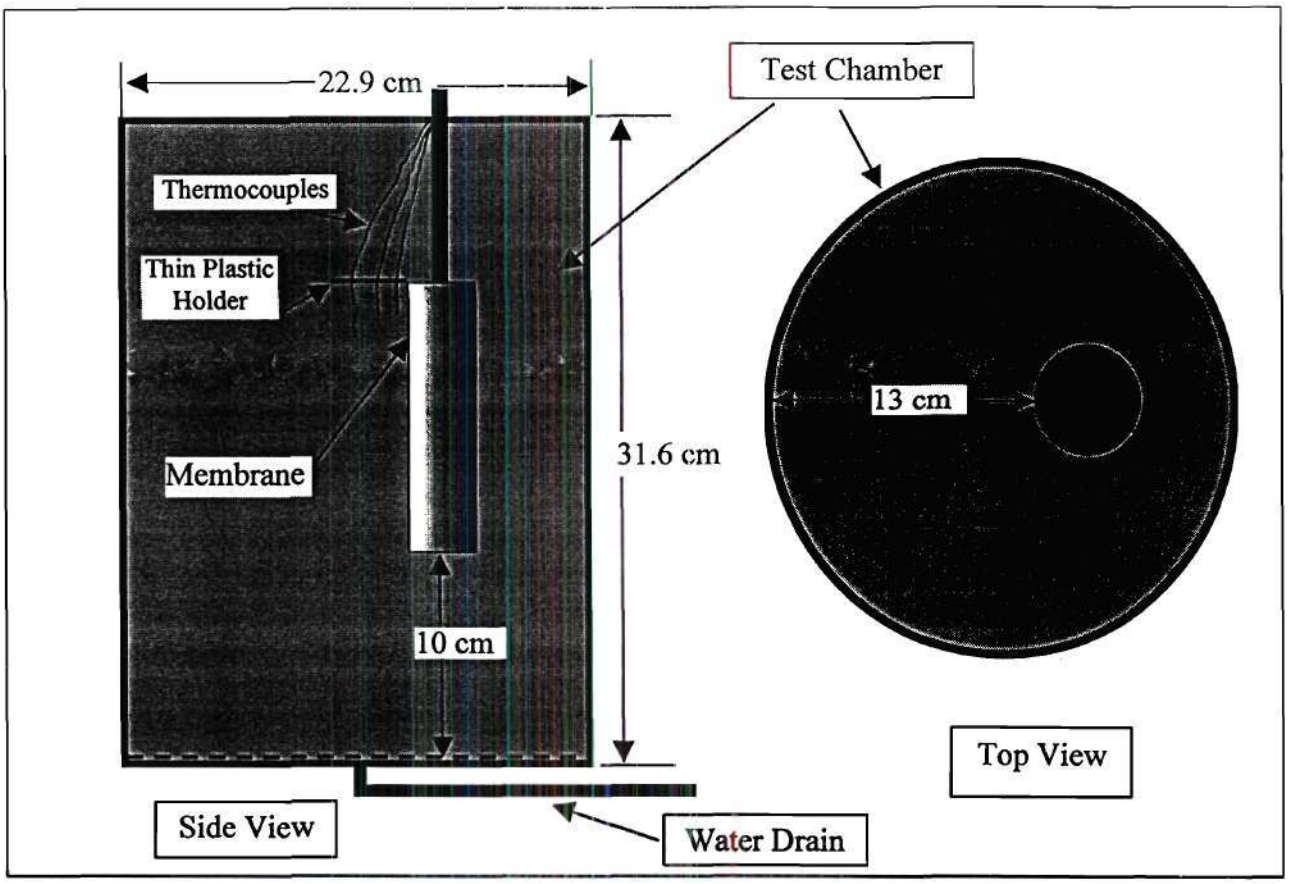

Figure 3.2 – MIP thermal influence test chamber.

Thermocouple temperatures were again recorded to ensure isothermal conditions, and then the membrane heater was engaged for a period of 10 minutes. The thermocouple temperatures were recorded at 0.3-second intervals for a total period of 30 minutes.

3.2 Task 2: Evaluation of VOC Mass Transfer from Contaminated Soil into the MIP

The structure and transport properties of the membrane were determined by measuring the rate of gas flux from the membrane induced from an external a transient and steady-state gas supply. Membrane transport characteristics were determined for three different gasses, over a

range of applied pressures and membrane temperatures. VOC mass transfer was evaluated by pumping water containing 50 mg/L trichloroethylene(TCE) through a 2mL chamber attached to the MIP. Mass transferred from gas, water, and water saturated sand for different membrane temperatures were used to determine mass separation factors from gas, water, and saturated soil.

3.2.1 Determining Membrane Transport Properties

Geoprobe® Systems creates the MIP membrane by heating (sintering) colloidal polytetrafluoroethylene (Teflon) powder into a stainless steel mesh screen. This process generally yields a micro-porous membrane structure with porosity from 10 to 40%, and an irregular pore structure with a wide range of pore sizes (Porter, 1990). Gas transport through micro-porous membranes can be described by Knudsen flow (Shelby, 1996), a type of pore diffusion where molecule-wall interactions dominate. However, sintering can also yield fully dense membranes where gas transport is described by diffusion solubility (Cussler, 1997). The apparatus shown in Figure 3.3 was used to evaluate the micro-porous nature of the membrane structure of the laboratory-scale MIP membrane. A block of acrylic (6cm wide by, 9cm long by 2.5cm deep) with a 2mL void (1.4cm diameter by 1.5cm deep) was clamped to the exterior of the MIP covering the membrane and a portion of the heater block. Gas pressure was then supplied to the 2mL void and the system was checked for gas leakage. Once the system was verified to be leak free, gas was supplied at a fixed pressure and allowed to flow through the membrane. The flow rate induced by a steady gas pressure was

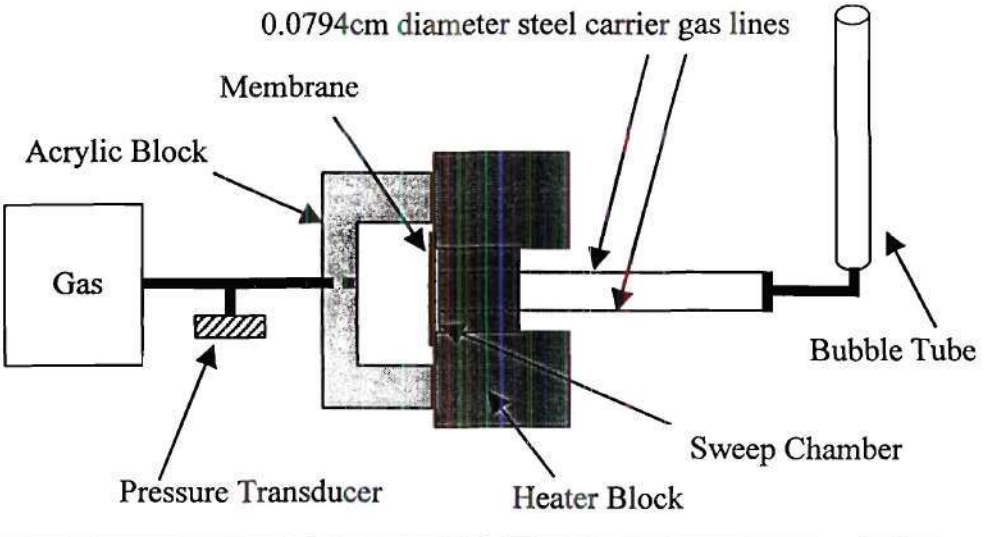

Figure 3.3 – Steady-state gas flow test apparatus.

measured by recording the travel time of a soap bubble traversing a fixed distance up a bubble tube. This experiment was repeated for a series of exterior gas pressures, at membrane temperatures, and with different gases, including air, helium, and carbon dioxide.

3.2.2 Diffusion Flow-Through Cell

A diffusion cell is an open system often used to measure pressure and temperature dependent fluxes for material samples placed between two flowing fluid streams (Figure 2). The diffusion cell has several advantages over a closed system including time invariant operation and control of the pressure drop across the material sample (Cunningham and Williams, 1980). The diffusion cell shown in Figure 3.4 was replicated by affixing an acrylic block to the exterior of the existing laboratory-scale MIP probe. The acrylic block, similar to the block used in the previous experiments, included a 1/8-inch inlet and outlet port that allowed water to be pumped through the 2ml void. The MIP was operated as if used for field application, which includes controlling the membrane temperature and flowing carrier gas past the interior side of the membrane. Known concentrations of VOCs in deionized water were then pumped past the exterior side of the membrane at a controlled pressure and flow rate.

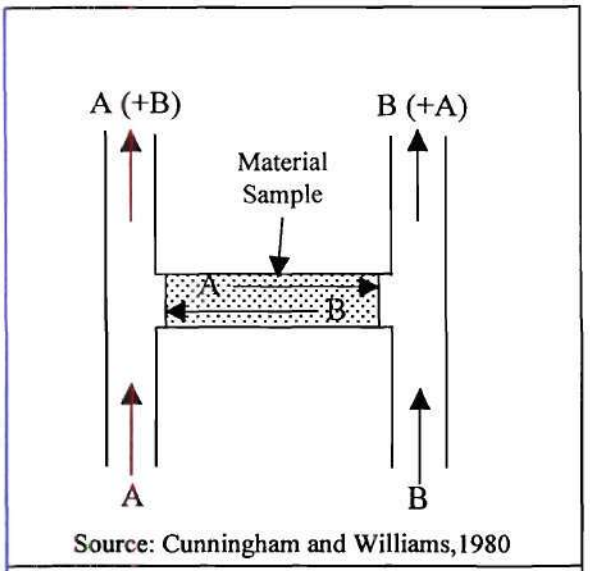

Source: Cunningham and Williams,1980

Figure 3.4 - Diffusion Cell Schematic

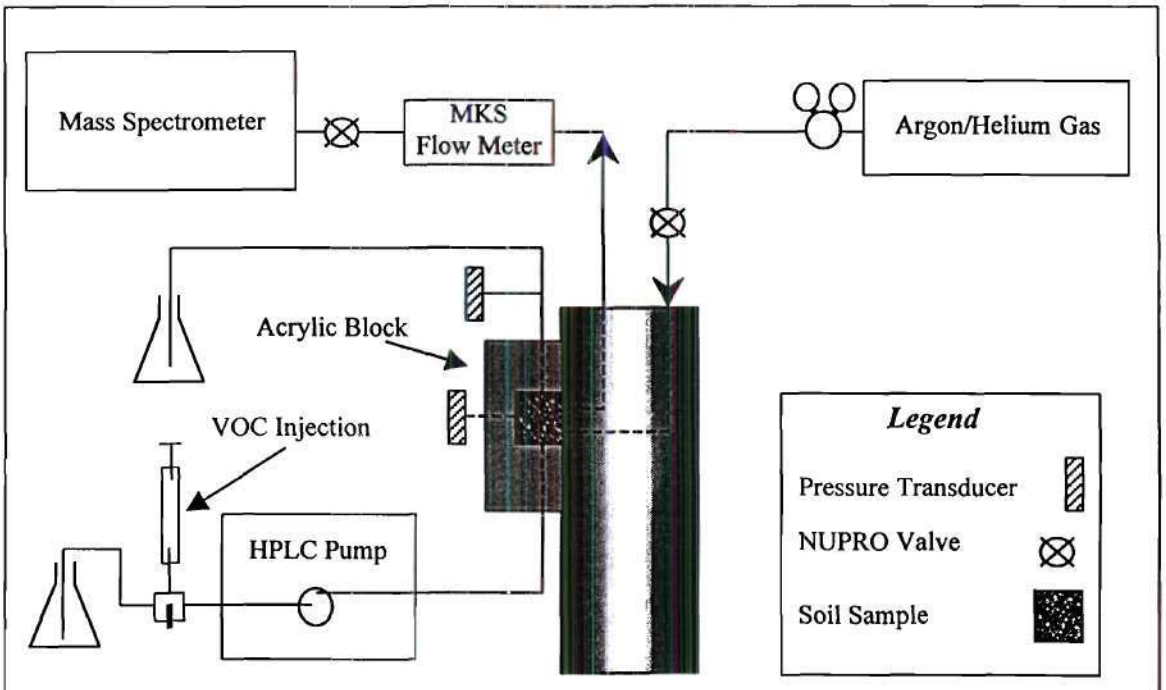

Figure 3.5 – Diffusion flow through cell process diagram.

Figure 3.5 shows the general layout of the diffusion cell experimental apparatus. The experimental procedure involved establishing a steady flow of helium/argon carrier gas interior to the membrane and a steady flow of VOC-free de-ionized water across the exterior of the membrane. Internal membrane carrier gas was supplied at a rate of 30mL per minute as indicated by an MKS model 1179 mass flow meter and at a pressure of 340 mbar (5 psi) as indicated by the analog pressure gauge within the Geoprobe® Systems model 2500 MIP controller. De-ionized water was supplied at a set flow rate using a Rainin model SD-200 pump with a Scientific Systems model LP-21 pulse damper. The de-ionized water flow rate was established at 5mL per minute, which resulted in approximately 34 mbar (0.5 psi) of fluid pressure exterior to the membrane as measured by a Honeywell 136 PC series Micro Switch model PK 8776 5 (0-15 psig range) pressure transducer. The de-ionized water flow-rate of 5mL per minute corresponds to approximately 1.67cm per minute of linear liquid velocity at the membrane face was chosen to provide constant VOC supply and simulate stagnant conditions. The standard cone penetrometer push rate is 60 to 120cm per minute (1 to 2cm per second or 2 to 4 feet per minute) for comparison. Steady-state fluid flows were established at a set membrane temperature indicated by the internal MIP K-type thermocouple and controlled through feedback by an OMRON model E5CS temperature controller within the Geoprobe® Systems model 2500 MIP controller.

The VOC laden carrier gas returned from the membrane was sent to the direct sampling Finnigan ITMS40 mass spectrometer. The ITMS was modified by Oakridge National Laboratories, Analytical Services Division. The ITMS is comprised of a quadrupole ion trap mass spectrometer, a capillary restrictor interface, and a variety of sample inlets for use with gas (air and soil gas), soil, and water. The system employed was a Finnigan ITMS 40 supplied by WSRC. The ITMS was fitted with a 20 cm long, 100 µm internal diameter capillary (J&W part #160-2635), and a restrictor heated interface (Scientific Information Service, Inc. part #912000) operated at 105°C. The capillary interface limits flow into the ITMS to 1% of the incoming gas flow rate, which is compatible with both electron impact (EI) and chemical ionization (CI) sources. Chlorinated solvents are analyzed using EI, whereas, benzene, ethyl benzene, toluene, and xylenes (BETX) are analyzed using water CI.

Once steady fluid flows and steady membrane temperature were achieved, the mass spectrometer was engaged to provide analysis of the carrier gas stream at one-second intervals. Approximately 200 seconds after initiating the mass spectrometer, water flow to the exterior of the membrane was switched from clean de-ionized water to a VOC solution at known concentration. The VOC solution was contained within a 60mL syringe that provided a constant contaminant supply for approximately 10 minutes. After the VOC solution was exhausted, water flow was switched back to clean de-ionized water while the mass spectrometer continued to analyze carrier gas effluent.

These experiments were completed for water only, at ambient (19°C) and operating (120°C) membrane temperatures. The experiment was repeated after filling the 2mL void within the acrylic block with 20-30 and then F-70 mesh Ottawa sand, and then with the membrane at ambient temperatures and at 40, 60, and 80°C.

3.3 Task 3: Assessment Soil Moisture Profiles using MRI

Georgia Institute of Technology Nuclear Magnetic Resonance (i.e., MRI) center has wide bore 9.4 Telsa magnet imaging system that can accommodate a non-electrically conductive sample within a 2.5-cm diameter tube in the temperature range from 0 to 120°C. The challenge was to construct a scale MIP model out of non-electrically conductive material that would have similar heat conduction properties as steel. Dr. Joe Cochran of the Materials Science and Engineering department recommended aluminum oxide ceramic as a material with heating characteristics similar to the tool steel used in the MIP. Common 0.6-cm diameter insulator tubes with 0.3-cm inside diameter (Scientific Instrument Services, Part #R10) were used to simulate the MIP and were placed in a 2.5-cm diameter borosilicate glass tube to simulate the MRI tube. The ceramic tubes were rapidly heated by passing 120°C water through the hollow center. This simple test showed that the temperature of the 2.5-cm borosilicate glass tube also rapidly reach 120°C.

It was concluded that the expense and effort involved in searching for an MRI instrument with larger diameter would not justify the experimental result. No further work was completed with MRI.

3.4 Task 4: Field Testing of the MIP for VOC Characterization

Two validation efforts were completed at the C Burning Rubble Pit located at SRS. The first field test was completed during the period 15 May through 18 May 2001 and was designed to collect baseline information used to direct laboratory experiments. The second field test was completed during the week of 4 through 7 September 2001. Both continuous and depth discrete sample collection methods were utilized, as well as collection of VOC samples at different membrane temperatures.

3.4.1 Initial Field Test

The WSRC MIP probe was used to complete all in-situ measurements. This full scale MIP was constructed by the U.S. Army Corps of Engineers, Waterways Experiment Station and is similar to the laboratory-scale MIP used in the bench-top experiments. A Geoprobe® Systems model 2500 MIP controller was used to control the MIP heater block and carrier gas flows. The WSRC direct sampling Finnigan ITMS40 mass spectrometer was used to analyze carrier gas returned during sample collection. The mass spectrometer and MIP were connected on 15 May and helium was used as the carrier gas at flow rate of 75mL/min as measured by a J&W Scientific ADM2000 Intelligent Flowmeter. Calibration standards for trichloroethylene and cis,-1,2-dichloroethylene were prepared and used per the U.S. Army Corps of Engineers, Tulsa District standard operation procedure (SOP No: M-0005-SWT-01) for calibrating the MIP and mass spectrometer. This involved preparing solutions of known concentration and mixing the solution with #2 blast sand within a jig that is affixed to the MIP membrane. The MIP and mass spectrometer were then operated to reproduce an in-situ measurement event resulting in a controlled analytic response to a known contaminant concentration. Dr. Joe Rossabi (WSRC) decided that a continuous, rather than a depth discrete sample collection mode would be more appropriate at the C Burning Pit because the

TCE contamination was present in a narrow vertical distribution that could have easily been missed by collecting samples at regular intervals. The standard calibration technique continued to be performed before and after each in-situ measurement to check for any equipment malfunctions. Continuous samples were collected from a total of seven (7) separate locations. The start time and depth along with the pauses between rod advancements were recorded to reconstruct the sample collection depth. The MIP heater block temperature and the return carrier gas pressure were recorded every one second using a Campbell CR23X data logger and a Honeywell 136 PC series Micro Switch model PK 8776 5 (0-15 psig range) pressure transducer. All in-situ analysis results were verbally communicated to Dr. Joe Rossabi and sent via email on 23 May 2001.

Dr. Rossabi returned to one of the continuous in-situ MIP sample locations (CPT-MIP-5) and collected continuous soil cores from ground surface to the depth where the CPT wireline sampler met refusal, which was near the beginning of the capillary fringe. Headspace analysis of the soil core samples by gas chromatography showed the presence of TCE at a depth similar to the location where the MIP and mass spectrometer had indicated the presence of TCE.

3.4.2 Second Field Test

The same equipment and configuration were used to complete the final field test. However, several modifications to the sample collection method were implemented based on the results of laboratory experiments. The standard Army Corp developed method of calibrating the MIP for depth discrete sample collection that involved spiking one liter of water and mixing with #2 blast sand was replaced with a method that used 0.01mL of 500mg/L TCE master stock solution injected onto the hot membrane. The master stock solution consisted of 7µL of neat TCE in 20 mL of HPLC grade methanol. This solution was prepared in the WSRC laboratory on 5 September 2001 before the field test began. The VOC drop method not only quantifies system response but also determines the exact carrier gas travel time from membrane to the mass spectrometer. This travel time is necessary to accurately determine the depth of sample collection. A second instrument check that consisted of injecting 100µL of gas collected by a gas tight syringe from the headspace of the 40mL vial that contained the 500mg/L TCE master stock solution. This instrument check was performed while the MIP was in the ground by injecting the gas sample into an injection port located on the Geoprobe® Systems model 2500 MIP controller. A final check on system performance was performed by using a carrier gas that contained 100 ppm of Argon gas. The Argon gas offers a continuous supply of constant concentration tracer used to evaluate membrane and mass spectrometer performance.

The final field test was conducted at the location previously found to contain a narrow vertical distribution of dissolved TCE (CPT-MIP-5). One continuous and two depth discrete sample collection efforts were performed near the continuous sampling effort completed in May 2001. The continuous sampling effort, whose purpose was to duplicate the previous effort, was completed with the MIP heater block temperature controller set to 120°C. A second sample collection effort involved sampling at discrete depths with the MIP heater block temperature controller set to 120°C. The third and final effort was designed to collect

samples from the same depths, but with the MIP heater block temperature controller set to 60°C. This temperature was chosen based on results of laboratory experiments.

4.0 Results and Discussion

Extracting VOCs from the subsurface by in-situ heating of soil with subsequent recovery through a membrane is a complex process. The following discussion of the experimental results is an effort to understand, at an operation level, some of the complexities involved with this sample collection process. This treatment is in no way exhaustive, but aimed at improving the state of knowledge and providing insights and recommendations for optimizing the sample collection process.

4.1 Task 1: Results of Temperature Profile Experiments

A series of ten experiments was conducted to assess the basic thermal influence of the MIP in porous media, and to provide the basis for future research efforts. The operating conditions and media used in these experiments are summarized in Table 4.1. Thermocouple data obtained for dry Ottawa sand (Experiment T-1) at four locations are shown in Figure 4.1.

Table 4.1 - Summary of conditions for temperature profile experiments.

Experiment	Porous Medium	Soil Moisture Condition	Thermocouple Placement
T-1	20-30 Sand	Dry	Internal Membrane Face 1 cm 3 cm 10 cm
T-2		Near Saturation Gravity Drained	
T-3	F-70 Sand	Dry Near Saturation Gravity Drained	
T-4		Gravity Drained Repeat Refilled Saturation Gravity Drained	
T-5	20-30 Sand	Dry and Near Saturation	
T-6		Gravity Drained	
T-7		Gravity Drained Repeat Refilled Saturation	
T-8	Appling Soil	Dry and Near Saturation	
T-9		Near Saturation Repeat Gravity Drained	
T-10		Gravity Drained Repeat	

The temperature within the membrane heater block as indicated by the internal thermocouple rapidly increased to approximately 120°C, and then oscillated over the 10-minute heating period in response to the "on-off" feedback controller with a set point of 120 °C. The temperature at the membrane surface also increased rapidly to approximately 110°C, but

exhibited dampened oscillations. The temperature recorded at the thermocouples located 1 and 3cm from the membrane showed very gradual increases to approximately 60°C and 32°C, respectively. The thermocouple located 10cm from the membrane remained essentially constant (~25°C) throughout the course of the experiment. These results indicate that the thermal influence under air dry soil conditions was much less than 10cm outward from the MIP. These data can also be used to estimate thermal soil properties (thermal conductivity) and heat transport due to moisture movement (Philip and DeVries, 1957).

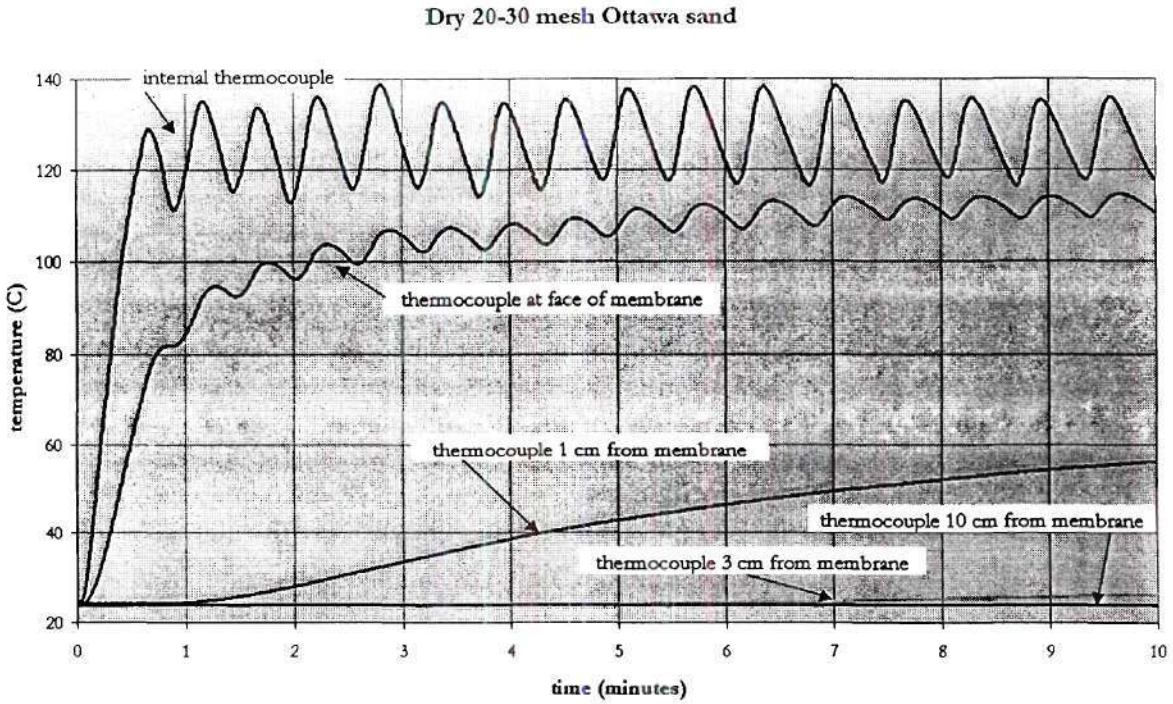

Figure 4.1 - Representative temperature responses for the laboratory-scale MIP buried in air dry 20-30 mesh Ottawa sand.

Commercial soil probes (Campbell Scientific model TCAV) utilize the rate of soil temperature increase to estimate soil thermal conductivity and moisture content. These devices are very thin (2-6 mm) and use a low wattage power supply (q = 1-2 W/cm) to gradually heat soil from approximately 20 to 80°C. Therefore, using the heat flow equation simplified by the Boussinesq approximations and assuming the Fourier's law of heat conduction applies:

$$\frac{DT}{Dt} = k\Delta^2 T \qquad (4.1)$$

The Equation 4.1 can be simplified since the probe gradually heats the surrounding soil uniformly about its circumference and over its entire length which leads to a relatively simple analytical solution (Healy et al., 1976):

$$T(a,t) = \frac{q}{4\pi\lambda}\ln\left(\frac{4kt}{a^2 C}\right) + T_0 \qquad (4.2)$$

where T is temperature, a is area, t is time, q is the heat released by the probe per unit length, λ is thermal conductivity, k is thermal diffusivity, and C is the soil heat capacity.

The MIP is over 4.5 cm in diameter and uses a 30 W/cm power supply to rapidly heat soil. Despite these differences relative to commercial soil probes, the applicability of the thin probe analytic solution (Equation 4.2) to the MIP thermal data was evaluated. Initially, a linear increase in temperature was recorded by the thermocouple located within the device (Figure 4.2). These data indicate that the thermal conductivity was greatest for the water-saturated 20-30 sand (smallest slope), and least for the dry 20-30 sand (greatest slope), with the gravity-drained 20-30 sand falling between these two extremes. Application of the analytical solution given in Equation 1 to these data yielded thermal conductivity values (λ) of 4.33, 4.45, and 4.74 W/m-C for the air dry, gravity-drained, and water-saturated 20-30 mesh Ottawa sand, respectively.

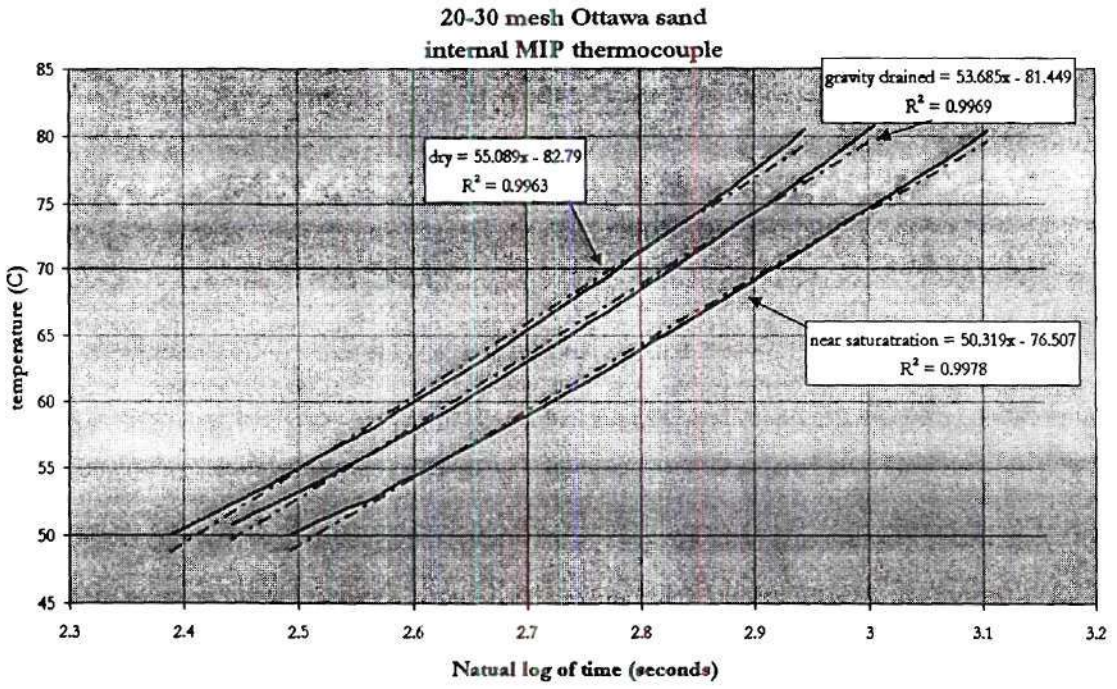

Figure 4.2 - Initial temperature increase recorded at the internal thermocouple within the laboratory scale MIP buried in air dry, water-saturated and gravity drained 20-30 mesh Ottawa sand.

Figure 4.3 shows the initial temperature increase obtained for F-70 Ottawa sand under similar moisture conditions. The thermal conductivity values obtained using Equation 1 for air dry, gravity-drained, and water-saturated F-70 Ottawa sand were 3.77, 1.26, and 2.17 W/m-C, respectively.

To evaluate the analytical solution given in Equation 4.2, a modified version of Equation 4.1 was developed using Cartesian coordinates for the flat heater block (see Figure 3.1). The modification, which assumes that velocity (u_x) is an inverse function of distance from the

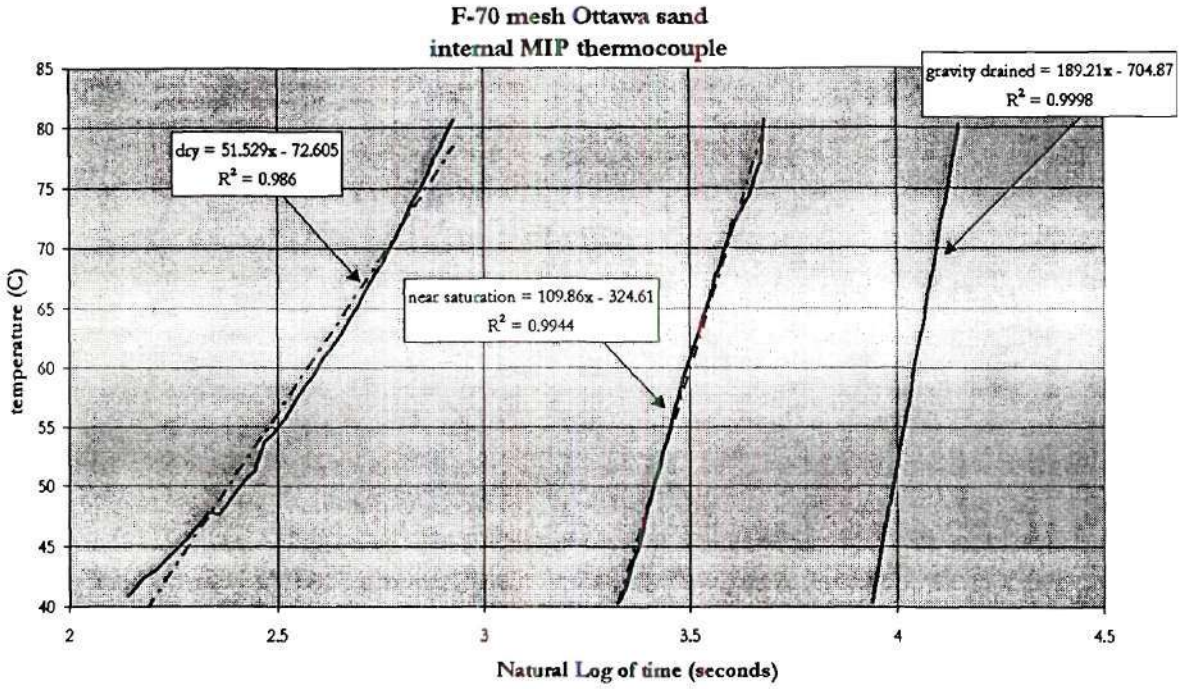

Figure 4.3 - Initial temperature increase recorded at the internal thermocouple with the laboratory-scale MIP buried in air dry, water-saturated and gravity drained F-70 Ottawa sand.

membrane (x), was based on the fit of all the experimental data to a finite difference solution (Equation 4.4)

$$\frac{\partial T(x,t)}{\partial t} = k\frac{\partial^2 T(x,t)}{\partial^2 x} - \frac{u_x}{x}\frac{\partial T(x,t)}{\partial x} \tag{4.3}$$

$$T(x,t+0.3) = \frac{k0.3}{(dx)^2}\left[T(x-dx,t) - 2T(x,t) + T(x+dx,t)\right] - \frac{u_x}{x}\left[T(x+dx,t) - T(x,t)\right] \tag{4.4}$$

Values for thermal diffusivity (k) and u_x were obtained when the sum of square differences between temperatures predicted at 1 and 3cm from the membrane by Equation 4.4, and temperatures measured at 1 and 3cm were minimized. The resulting fit of the Equation 4.4 to the temperature data obtained for wet 20-30 mesh Ottawa sand is shown in Figure 4.4. Thermal diffusivity (k) is related to thermal conductivity by $\lambda = k\rho C_p$. Based on input values for soil bulk density and specific heat, thermal conductivity values of 0.226, 2.46, and 1.83 cm^2/s were obtained for air dry, gravity-drained, and water-saturated 20-30 Ottawa sand, respectively. Thermal conductivity values estimated for each soil and water content are summarized in Table 4.2.

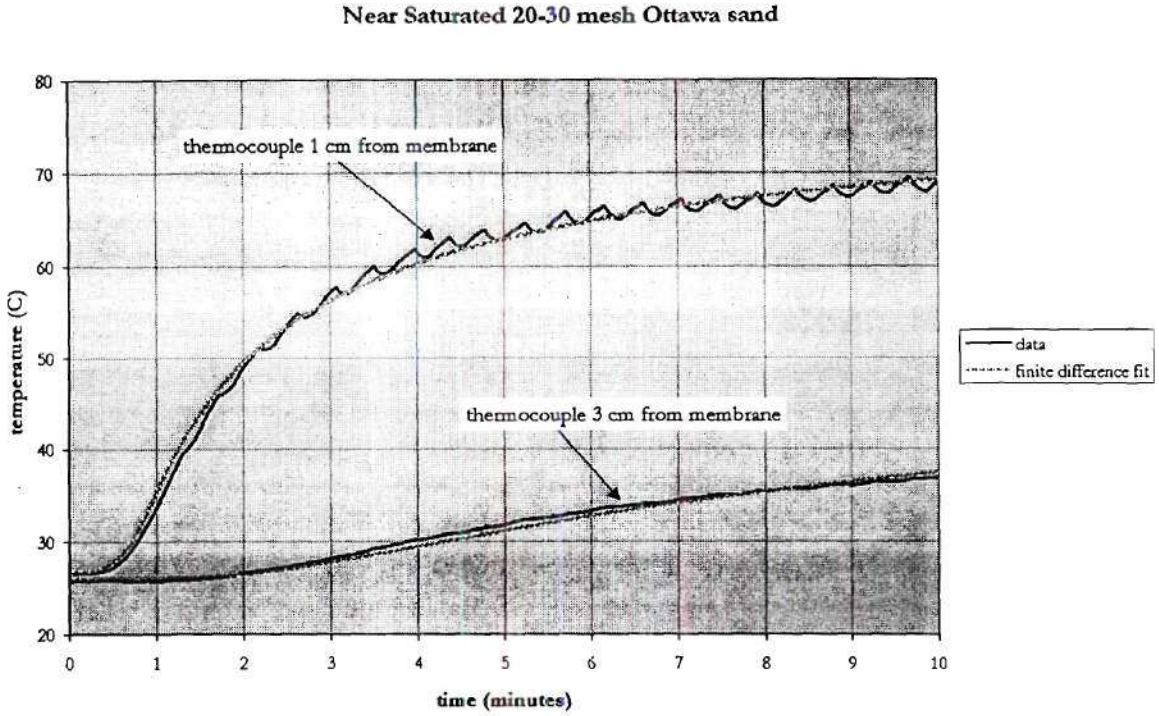

Figure 4.4 - Temperature recorded at thermocouples located 1- and 3-cm from the membrane and corresponding numerical (finite difference method) approximation.

Table 4.2 - Comparison of simulated and measured thermal conductivity values.			
Soil Condition	Thermal Conductivity (W/m-°C) (Analytical Solution: Internal MIP Thermocouple)	Thermal Conductivity (W/m-°C) (Finite Difference Method: External Thermocouples)	Thermal Conductivity (W/m-°C) (Published Values[a])
20-30 mesh Ottawa sand			
Air Dry	4.76	0.226	0.5 ± 0.3
Gravity Drained	4.98	2.46	1.3 ± 0.8
Near Saturation	5.19	1.83	2.2 ± 1.0
F-70 mesh Ottawa sand			
Air Dry	3.76	0.075	0.167
Gravity Drained	1.26	2.18	2.22
Near Saturation	2.17	2.49	--
Appling Soil			
Air Dry	4.13	0.289	0.36 ± 0.3
Gravity Drained	4.21	1.05	0.9 ± 0.9
Near Saturation	4.28	1.67	1.49 ± 1.0

[a]Edwards (1969)

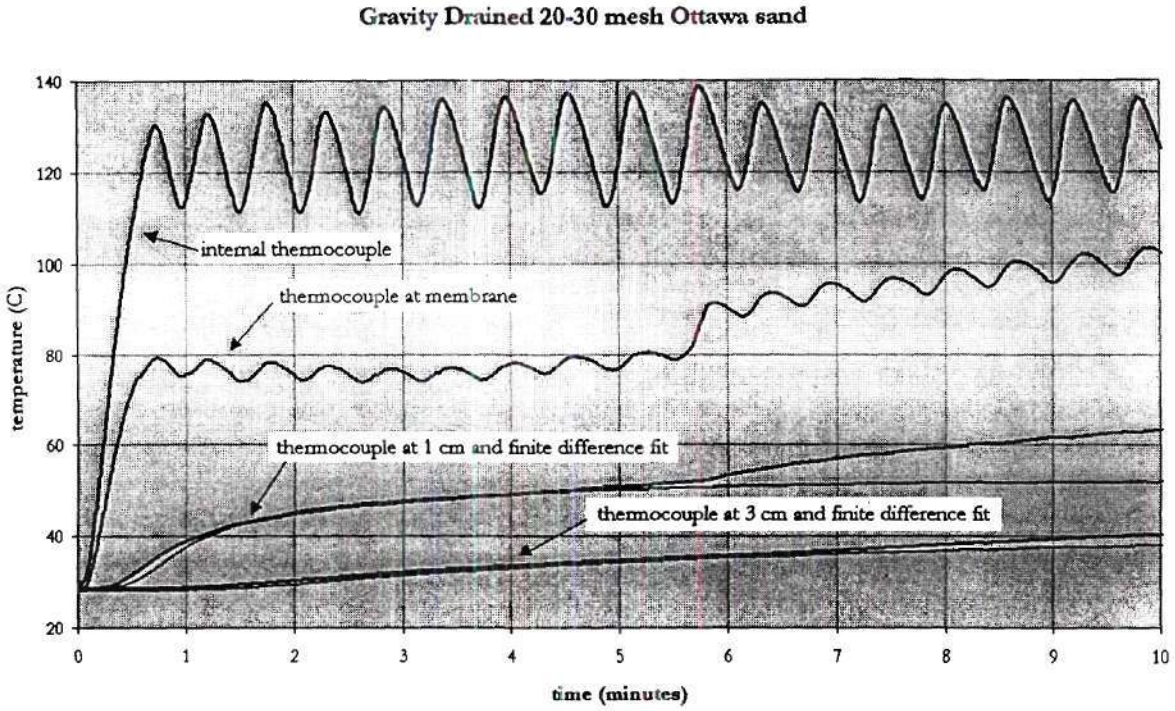

Figure 4.5 - Temperature recorded at thermocouples located within the MIP, at the membrane surface, and 1 and 3cm from the membrane. Also shown are the numerical (finite difference method) approximations of temperatures at 1 and 3cm from the membrane.

The measured soil temperature profiles for 20-30 and F-70 mesh Ottawa sand, and Appling soil at air dry, gravity-drained, and water-saturated conditions were similar to those shown in Figures 4.1 through 4.4. However, the measured temperature profile for gravity drained 20-30 mesh Ottawa sand was unique. Figure 4.5 shows the temperature recorded at the internal thermocouple indicate that the device achieved operating temperature (120°C) within one minute while the thermocouple located at the membrane surface didn't reach 100°C until after 8 minutes had elapsed. The membrane surface temperature reached 100°C within 1-minute for gravity-drained F-70 and Appling soils, and all water-saturated soils. The step increase that occurred after 5 minutes of heating (Figure 4.5) is probably due to preferential soil drying, which has been shown to occur adjacent to underground electrical transmission cables (Couvillion, 1982).

In summary, the results of the temperature profile experiments demonstrate that the internal MIP thermocouple temperature cannot be used to directly infer external soil temperature. This is particularly evident for the gravity-drained 20-30 Ottawa sand where the temperature on the membrane surface was approximately 40°C lower that indicated by the internal MIP thermocouple temperature. Soil thermal properties cannot be determined using Equation 4.2. This is evident from the lack of agreement between the thermal conductivties determined by Equation 4.2 using the internal MIP thermocouple temperature and thermal conductivities obtained by the finite difference fit of measured external temperatures (Table 4.2). Results also show that significant thermal influence does not extend beyond 1cm from the membrane.

4.2 Task 2: Evaluation of VOC Mass Transfer from Contaminated Soil into the MIP

An initial series of experiments that involved applying pressurized gas on the membrane exterior and measuring the rate of gas flux from the membrane was performed to determine the membrane transport mechanisms and effective transport properties. The gases used included helium, carbon dioxide, and air, which were applied at external pressures ranging from 0.1 to 2.5 bar of gauge pressure. VOC mass transfer was evaluated by pumping water containing 50 mg/L trichloroethylene(TCE) through a 2mL chamber attached to the membrane exterior. Mass transferred from gas, water, and water saturated sand for different membrane temperatures was measured, and used to determine membrane separation factors (from gas) and pervaporation separation factors (from water and water-saturated soil).

4.2.1 Transport Mechanism

Possible mass transport mechanisms in membranes include viscous flux or flow in capillaries, Knudsen diffusion where molecule-wall interactions predominate, and solution-diffusion involving an adsorpotion step before intramembrane transport by diffusion. Membranes constructed by sintering are normally micro-porous (Shelby, 1996 and Porter, 1990) and transport can be described by the Hagen-Poiseuille equation modified for porous media:

$$J_v = -\frac{B_v}{\mu}\frac{P}{RT}\frac{dP}{dx} \qquad \text{Cunningham and Williams, 1980 (4.5)}$$

or as Knudsen diffusion:

$$J_k = -D_{ij}^K \frac{1}{RT}\frac{dP}{dx} \qquad \text{Cunningham and Williams, 1980 (4.6)}$$

where J is the molar flux (moles/cm^2-s), B_v is the viscous permeability, P is the gas pressure, R is the gas constant, T is absolute temperature, x is the membrane thickness, μ is the gas viscosity, and D^K is the Knudsen diffusion coefficient. Figure 4.6 illustrates that the total flow of gas through a membrane is a combination of both Poiseuille capillary flow and Knudsen diffusion. However, at low applied pressures, Knudsen diffusion tends to be the predominant mechanism.

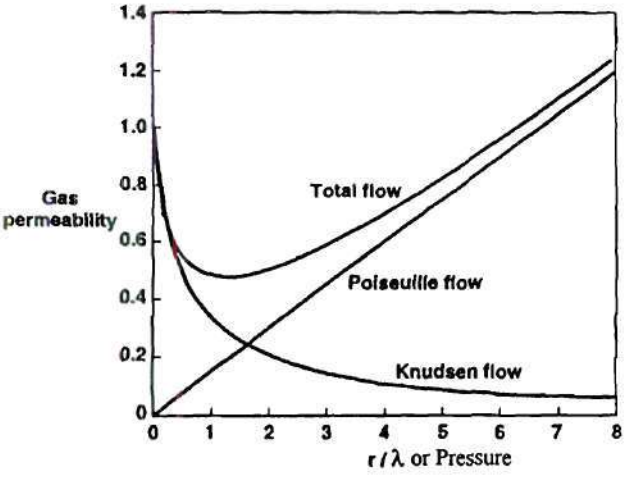

Figure 4.6 Illustration of the proportion of Knudsen to Poiseuille flow as a function of r/λ or Pressure.
Source: Baker, 2000

Transient or time variable and steady-state flow measurements are commonly used to determine membrane transport properties. Shelby (1996) suggests monitoring the decay of a pressure pulse into micro-porous membranes to determine permeability, and to

distinguish any pressure dependence. A plot of the natural log of pressure difference across the membrane with time should be linear for Knudsen diffusion (Equation 4.7), while a plot of the inverse of applied pressure with time will yield a straight line for viscous advective flux (Equation 4.8).

$$\ln \Delta P = -\frac{B_k}{l} t - \ln \Delta P_0 \quad \text{Knudsen Diffusion} \qquad (4.7)$$

$$\frac{1}{P} = \frac{B_v}{2l} t - \frac{1}{P_0} \quad \text{Viscous Flux} \qquad (4.8)$$

where B_k is the Knudsen permeability and B_v is the viscous permeability (mol/cm-bar-s), l is the membrane thickness (~0.1cm), ΔP_0 is the pressure difference at initiation.

Figure 4.7 shows the pressure decay for an initial 2.5-bar pulse of helium and carbon dioxide gas through the membrane plotted as the natural log of the pressure difference across the membrane. As shown on Figure 4.7, helium appears to fit the equation describing Knudsen diffusion since there is a linear decay of the natural log of the pressure difference across the membrane with time. However, carbon dioxide exhibits non-linearity in the initial 50 seconds which corresponds to from 2.5 to 1 bar applied pressure, but is linear from approximately 80 seconds on or in the 0.58 to 0.1 bar region.

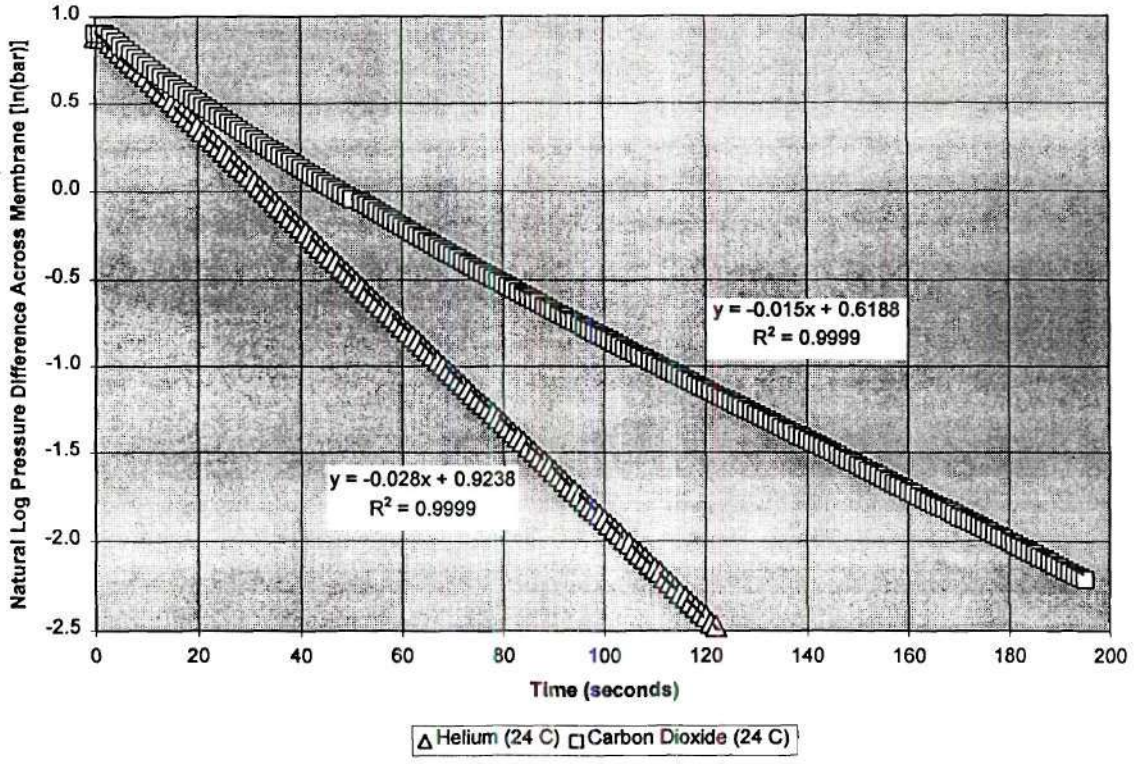

Figure 4.7 – Plot of the natural log of pure gas pressure applied across the laboratory scale MIP membrane. Plot shows the decay of an initial 2-bar pressure pulse with time.

The pressure decay for an initial 2.5-bar pulse of helium and carbon dioxide gas through the membrane plotted as the inverse of the applied pressure is shown in Figure 4.8. Helium permeability does not appear to be a linear function of inverse pressure while carbon dioxide permeability was linear over the 2.5 to 1 bar pressure range. Helium transport through the membrane is consistent with the Knudsen diffusion mechanism (Equation 4.7) from to 0.1 to 2.5 bar pressure range. Carbon dioxide transport is consistent with viscous flux mechanism (Equation 4.8) in the 2.5 to 1 bar range and Knudsen diffusion in the 0.58 to 0.1 bar pressure range. Carbon dioxide transport within the membrane transitions from Knudsen diffusion to viscous flux as shown in Figure 4.1 depending on the applied pressure, while helium displays pure Knudsen diffusion via this transient experimental technique.

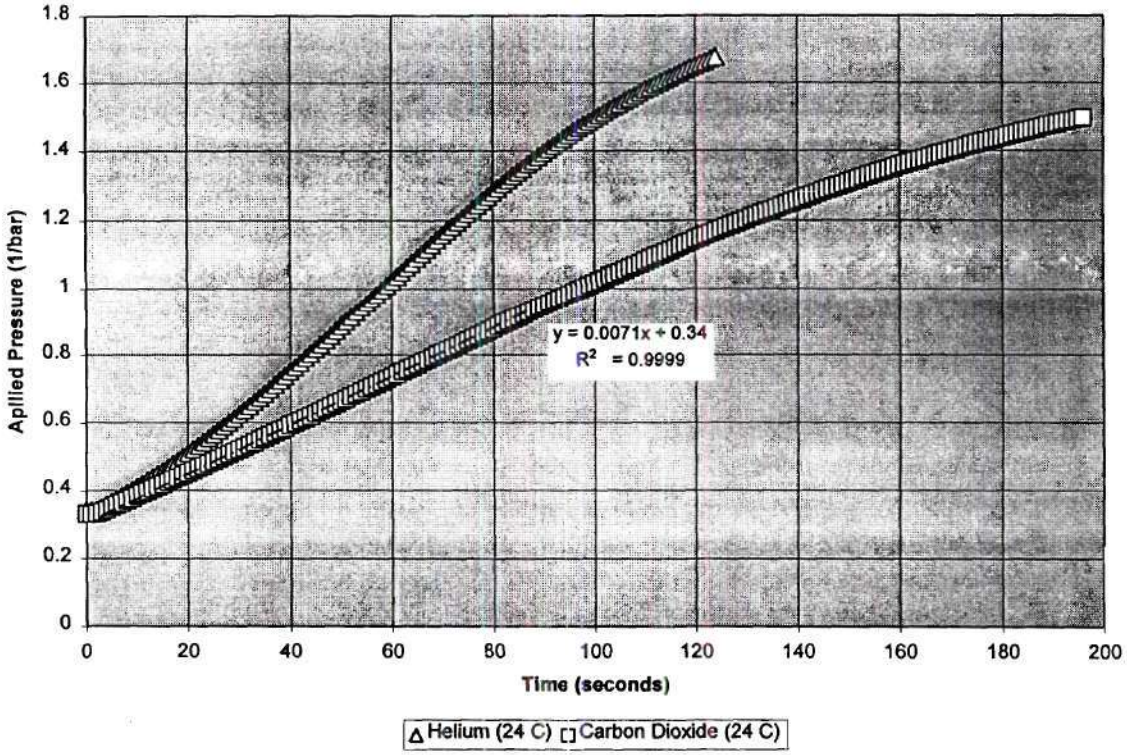

Figure 4.8 - Plot of the inverse of the total pressure of a pure gas applied to the laboratory scale MIP membrane. Plot shows the decay of an initial 2-bar pressure pulse with time.

A second experiment involved measuring the flow of gas out of the membrane in response to a constant pure gas pressure. The results of measured gas flow for helium, air, and carbon dioxide are shown in Figure 4.9. Helium flux exceeded that of carbon dioxide and air in the 0.1 to 0.9 bar pressure range. This behavior is opposite of that predicted by Equation 4.5, which shows that the difference between molar flux is primarily dependent on differences in the inverse of viscosity's at similar pressures and temperatures. Helium has a higher viscosity than carbon dioxide or air (20, 15, 18.5μP at 24°C respectively), if gas flow can described by Equation 4.5, carbon dioxide should have the largest flux, followed by air, and then helium. The observed response shown in Figure 4.9 is opposite of that predicted by Equation 4.5, therefore, gas flow through the membrane can't be described by viscous flux mechanisms.

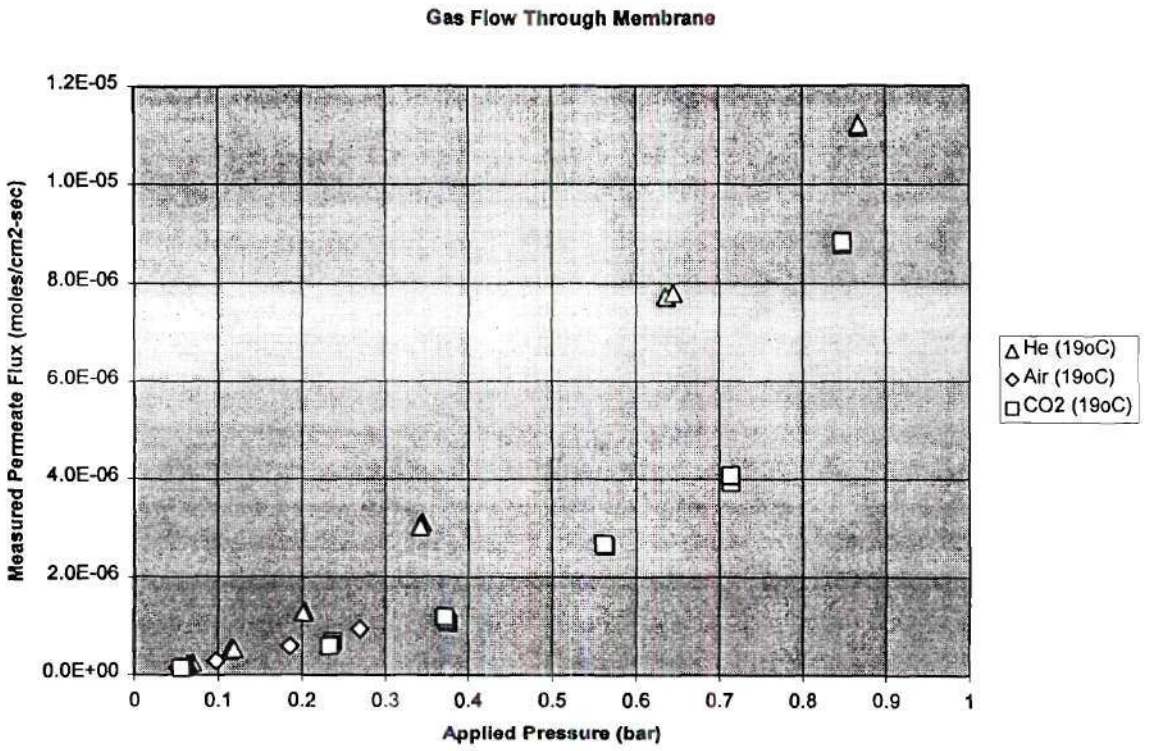

Figure 4.9 – Gas flux from the membrane resulting from a steady pressure applied across the membrane. Applied pressure is gauge pressure.

The results of the first gas flow experiment shown in Figures 4.7 and 4.8 show that gas flow through the membrane is consistent with Equation 4.7 which describes Knudsen diffusion for transient applied pressures. Equation 4.6 has to be used to demonstrate that Knudsen diffusion applies to the results shown in Figure 4.9, this requires a description for the Knudsen diffusion coefficient which is given by Cussler (1997) as:

$$D_{ij}^{K} = \frac{d}{3}\left[\frac{2RT}{mw}\right]^{1/2} \tag{4.9}$$

where mw is the molecular weight and d is the mean pore diameter. Combining Equation 4.6 with 4.9 yields the flux term:

$$J = -\frac{d}{3}\sqrt{\frac{2}{RTmw}}\frac{dP}{dx} \tag{4.10}$$

which predicts that the difference in flux between pure gases is dependent on the square root of the ratio of molecular weights, commonly known as Graham's square root law for diffusion in porous media:

$$\frac{J_{He}}{J_{CO2}} = \sqrt{\frac{mw_{CO2}}{mw_{He}}} \tag{4.11}$$

Results of Figure 4.7 and 4.8 show that that helium and carbon dioxide gas flow through the membrane is consistent with Knudsen diffusion for pressures below approximately 0.5 bar. Figure 4.10 shows the measured flux from Figure 4.9 in the 0.05 to 0.4 bar pressure range..

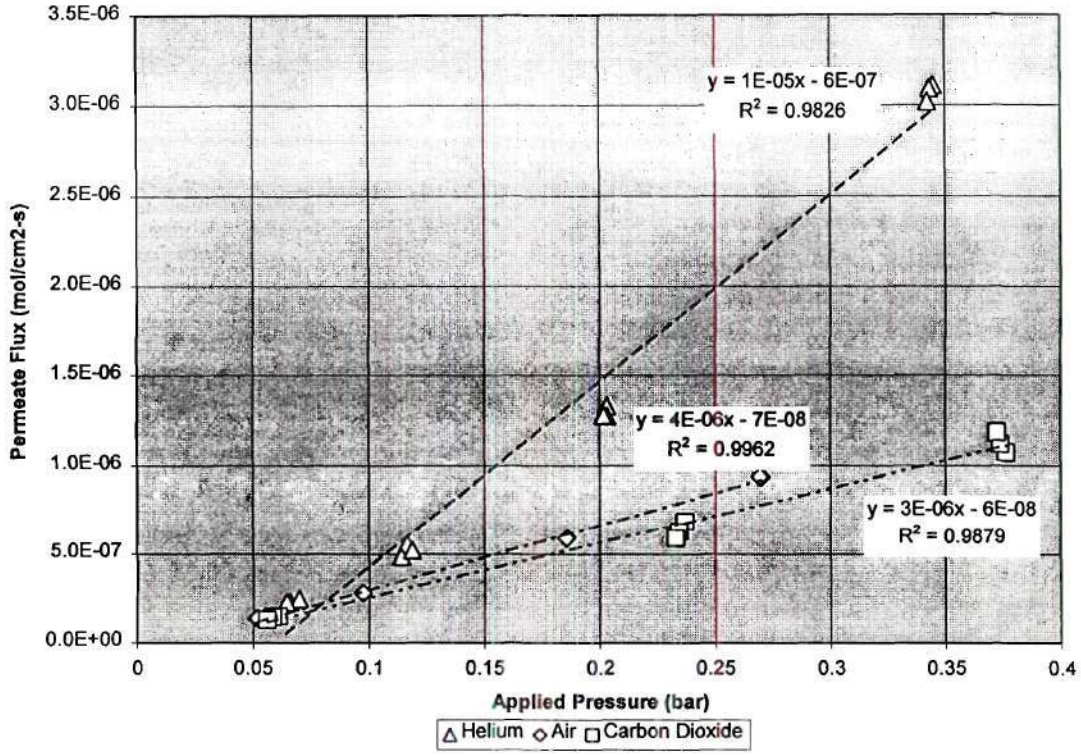

Figure 4.10 – Gas flux from the laboratory-scale MIP membrane resulting from a steady pressure applied across the membrane.

Table 4.3 shows the slope calculated from the linear regression of flux vs pressure for the data shown in Figure 4.10, the ratio of the calculated slopes for each gas pair, and along with the square root of the molecular weight ratios (Graham's law, Equation 4.11). The measured flux ratios are in good agreement with the Graham's law ratios, which shows that Equation 4.11 applies, meaning that Equation 4.10 can be used to describe gas flow through the membrane in the 0.05 to 0.4 bar pressure range. Gas flow through the membrane can be described as Knudsen diffusion.

Table 4.3 – Comparison Between Measured Flux Ratios and Graham's Law Ratio					
Gas	Slope of Flux vs Pressure	Molecular Weight	Gas Pair	Slope Ratio	Graham's Law Ratio
Helium	1.043×10^{-5}	4	He/CO_2	3.35	3.32
Carbon Dioxide	3.110×10^{-6}	44	He/Air	2.82	2.68
Air	3.701×10^{-6}	28.8	CO_2/Air	0.84	0.81

4.2.2 Membrane Transport Properties

Both the transient and steady-state experimental results indicate that Knudsen diffusion can be used to describe gas flow at low applied pressure. The Knudsen diffusion coefficent can be determined from the slope given in Table 4.3:

$$D^K = slope RTl \qquad (4.12)$$

where l is the membrane thickness (~ 0.1cm). The measured Knudsen diffusion coefficient can then be used to estimate the mean pore diameter from:

$$d = D^K \frac{mw}{4850\sqrt{T}} \qquad \text{Cussler, 1997 (4.13)}$$

where 4850 was obtained from an exact kinetic theory calculation. Table 4.4 shows the diffusion coefficients determined by Equation 4.12 and Figure 4.10, and the mean pore diameter from equation 4.13.

Table 4.4 – Membrane Properties

Gas Species	D^K (cm^2/s)	Pore diameter (cm) Equation (4.13)	Mean Path Length (cm) (CRC 82nd ed.)	Kn #
Helium	0.025	$1.2x10^{-6}$	$20.00x10^{-6}$	16.67
Air	0.009	$3.1x10^{-6}$	$6.91x10^{-6}$	2.23
Carbon Dioxide	0.0075	$4.0x10^{-6}$	$4.51x10^{-6}$	1.13

Figure 4.6 also included a d/λ parameter along the ordinate (the ratio of the membrane pore diameter to the molecular mean free path), which is the inverse of the Knudsen number (Cunningham and Williams, 1980, Cussler, 1997, and Baker, 2000). The Knudsen number is another method used to help distinguish between viscous flux and Knudsen diffusion. The mean free path lengths given in Table 4.4 are for gases at atmospheric pressure and 25°C. There is no general consensus on interpretation of Knudsen numbers, but molecular collisions with the pore walls are considered to be more prevalent at larger Knudsen numbers (Baker, 2000).

The mean membrane pore size obtained from this analysis (12 to 40 nm) are classified as mesopores based on the IUPAC classification scheme (Choi, 2001). Surface and capillary forces can play an important role in mesopores. As a result, the sintered teflon membrane used in the MIP may exhibit behavior such as surface diffusion and possibly capillary condensation that are currently not well defined membrane phenomenon.

Cunningham and Williams (1980) show that the ratio of Knudsen diffusion coefficient to the free molecular coefficient represent an obstruction factor (Q_p), which is directly related to the

fraction of gas allowed to enter the membrane. Table 4.5 contains the free gas diffusion coefficient for each gas into air and the corresponding obstruction factor.

Table 4.5 – Membrane Obstruction Factor			
Gas Species	D^K (cm^2/s)	$D_{i\text{-}air}$ (cm^2/s)*	Obstruction Factor Q_p ($D^K/D_{i\text{-}air}$)
Helium	0.025	0.696	0.036
Air	0.009	0.199	0.045
Carbon Dioxide	0.0075	0.162	0.046
			*Grigoriev et al., 1997

The relative magnitudes of the obstruction factors are not surprising since helium has the largest free mean path, followed by air, and carbon dioxide (Table 4.4). The larger the free mean path, the lower the probability of the molecule entering the pore.

An alternative expression for the Knudsen diffusion coefficient (Equation 4.9) is given by Choi et al., (2001):

$$D^K = n\tau\frac{d}{3}\left(\frac{8RT}{\pi mw}\right)^{1/2} \quad \text{rearranged to give:} \quad n\tau = \frac{3D^K}{d}\left(\frac{\pi mw}{8RT}\right)^{1/2} \tag{4.14}$$

where n is the membrane porosity and τ is the membrane tortuosity. The membrane porosity to tortuosity can be calculated using Equation 4.14 using the measured Knudsen diffusion coefficients given in Table 4.5. Cunningham and Williams (1980) note that the membrane obstruction factor is equal to the membrane surface porosity multiplied by tortuosity ($n = Q_p\tau$), which can be combined with the calculated $n\tau$ from Equation 4.14 to yield the membrane toruosity:

$$n\tau = A \text{ from Equation 4.14, and } n = Q_p\tau \text{ which becomes } \tau = \sqrt{\frac{A}{Q_p}} \tag{4.15}$$

Once the tortuosity is calculated from Equation 4.15, the membrane porosity can then be calculated from Equation 4.14. Table 4.6 shows the porosity tortuosity calculated for each gas using Equation 4.14 and the Knudsen diffusion coefficients given in Table 4.5, the calculated tortuosity using Equation 4.15, and the porosity calculated from Equation 4.14.

Table 4.6 – Membrane Porosity			
Gas Species	Porosity Tortuosity Equation 4.14	Tortuosity Equation 4.15	Porosity
Helium	0.51	3.71	0.135
Air	0.19	2.03	0.093
Carbon Dioxide	0.15	1.80	0.083

The obstruction factor in Table 4.5 suggests that helium was relatively less likely to enter the membrane pores. However, the porosity calculated from helium results (Table 4.6) is the largest of the three values and the tortuosity the smallest. There are two possible explanations that fit these observations, one is that helium progress, once inside the membrane pores, is unimpeded and fully explores the membrane structure. The other explanation is that in addition to the Knudsen diffusion, helium is undergoing solution-diffusion through the teflon spheres.

The membrane within the laboratory-scale MIP has a mean pore diameter that ranges from 122 to 400 angstroms. The portion of the membrane surface area available for gas transport ranges from 3.6 to 4.6%.

4.2.3 Results of Mass Transfer Experiments

Pervaporation describes a membrane separation process in which a multicomponent liquid feed is passed across the exterior of a membrane while a partial vacuum is maintained on the interior side of the membrane. Some liquid species preferentially permeate through the membrane and enter the gas phase. Maintaining a low interior vapor pressure relative to the membrane exterior drives the process. The pervaporation process can be divided into two steps, the evaporation of the feed liquid to form a saturated vapor in contact with the membrane exterior, and diffusion of the vapor through the membrane. (Baker, 2000)

The flux of permeating species entering the interior side of the membrane can be expressed as:

$$J = D^{K} \frac{(p_{io} - p_{il})}{lRT} \tag{4.16}$$

where D^K is the Knudsen diffusion coefficient, p_{io} is the vapor pressure of the permeate species on the external side of the membrane, p_{il} is the internal vapor pressure, and l is the membrane thickness. The internal permeate vapor pressure can be effectively ignored for most of the dilute solutions encountered during operation of the MIP and because the membrane interior side is continuously swept with a carrier gas. Therefore, the main driving force for solute transport across the MIP membrane is the vapor pressure of the species in equilibrium with the exterior of the membrane. For most dilute concentrations of VOCs the subsurface vapor pressure can be described by Henry's law and related to the membrane flux by:

$$J = D^{K} \frac{K_H C_i}{lRT} \tag{4.17}$$

Where K_H is the temperature dependent Henry's coefficient and C_l is the aqueous phase concentration of the VOC species. Combining Equations 4.9 and 4.17 yields:

$$J = -\frac{d}{3l}\sqrt{\frac{2}{mwRT}}K_H C_i \qquad (4.18)$$

The temperature dependent Henry's coefficient was determined for trichloroethylene (TCE) by Heron, et al. (1998) for a maximum temperature of 95°C:

$$K_H = \exp(186.10 - \frac{12540}{T} - 26.11\ln T) \qquad (4.19)$$

where K_H is in atm m^3/mol. Equations 4.18 and 4.19 can be combined to yield an expression that is temperature dependent in both numerator and denominator. Figure 4.11 shows a plot of predicted flux of TCE through the membrane from an aqueous solution containing 50 mg/L of TCE using Equations 4.18 and 4.19 with increasing membrane temperature. The flux peaks at 100°C at the maximum Henry's coefficient and decreases due to gas expansion (1/T).

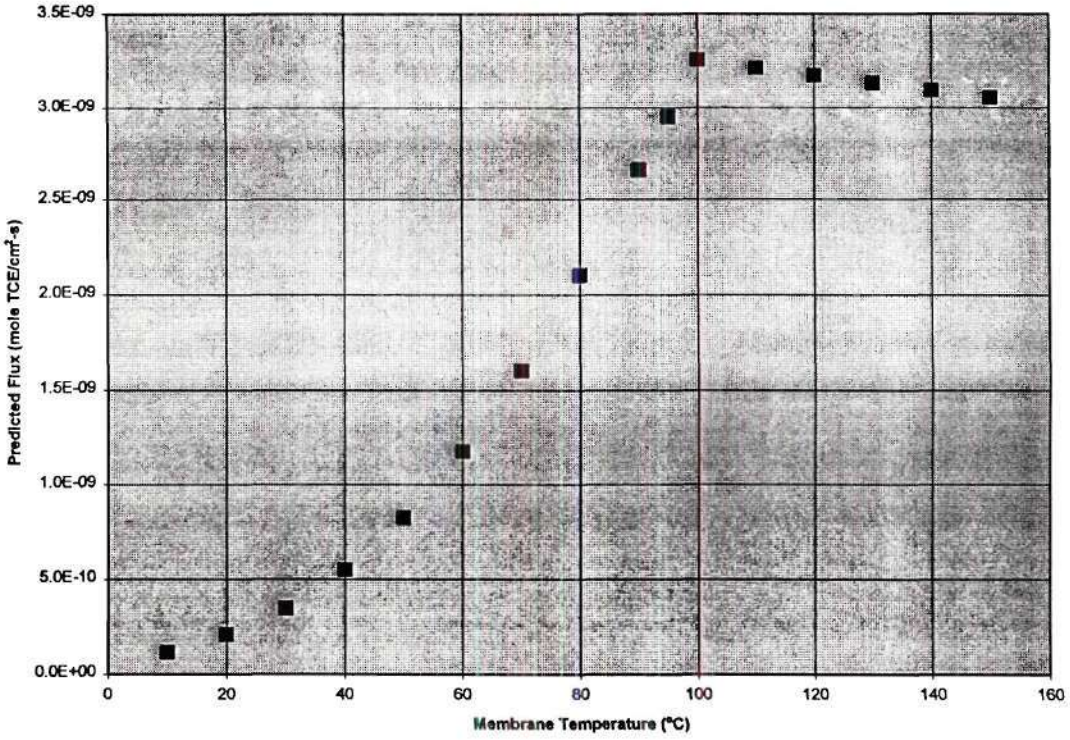

Figure 4.11 – Predicted TCE flux through a membrane by pervaporation description using a temperature dependent Henry's coefficient.

Membranes used for Pervaporation are usually described by their selectivity to particular solutes of interest over unwanted solvents. The purpose of the MIP membrane is to selectively remove VOC contaminants from the subsurface environment. This requires the determination of both gas and aqueous phase selectivity to adequately describe operation of the MIP membrane. The gas phase selectivity is describe by the membrane separation factor given as:

$$\beta_{membrane} = \frac{p_{il} / p_{jl}}{P_{io} / P_{jo}} \qquad \text{Baker, 2000} \qquad (4.20)$$

where P_{il} and P_{jl} are the vapor pressures of the solute and solvent on the interior side of the membrane, and P_{io} and P_{jo} are the vapor pressures of the solute and solvent in equilibrium with the exterior of the membrane. The aqueous phase selectivity is described by the overall pervaporation separation factor given as:

$$\beta_{pervap} = \frac{p_{il} / p_{jl}}{C_{io} / C_{jo}} \qquad \text{Baker, 2000} \qquad (4.21)$$

where , and C_{io} and C_{jo} are the aqueous phase concentrations of the solute and solvent in equilibrium with the membrane exterior. Figure 4.12 shows a plot of trichloroethylene (TCE) and water ions detected by direct mass spectrometer analysis of the carrier gas. This data was obtained by placing the heated MIP over a small volume of 50 mg/L TCE solution so that membrane was the only migration pathway for vapors. Also plotted on Figure 4.12, is the membrane separation factor calculated for each analysis result using Equation 4.20. The mass spectrometer determines the abundance of each ion in the carrier gas and is directly proportional to the ion's vapor pressure. TCE is reported as ion 132 and water is reported as ion 18. The membrane separation factor was determined by:

$$\beta_{membrane} = \frac{\text{Ion 132 Abudance/Ion 18 Abundance}}{K_H C_{TCE\,l} / \text{Vapor Pressure of } H_2O} \qquad (4.22)$$

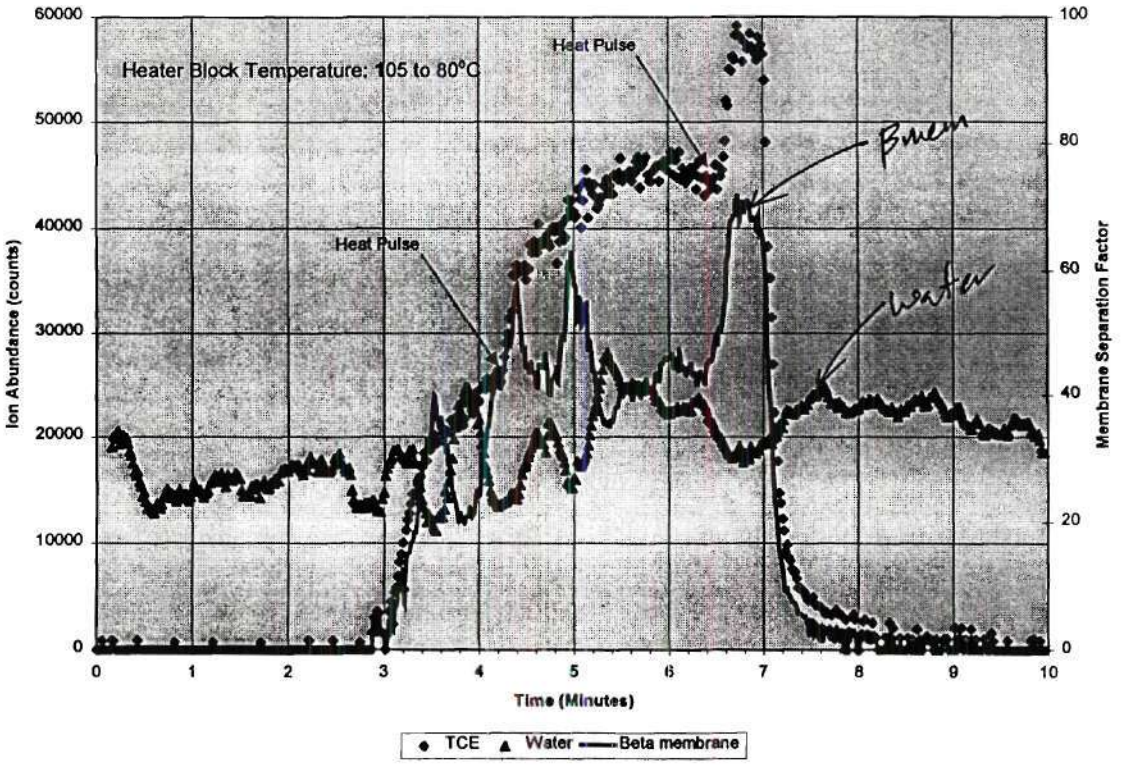

Figure 4.12 – Transfer of TCE and water from the headspace of a 50 mg/L solution with the MIP operating between 80 and 105°C.

A primary assumption used for determining the membrane separation factor was that the membrane and water are at the temperature indicated by the thermocouple located in the membrane heater block. These experiments were completed after waiting for the MIP heater block to reach a stable temperature, but there was at least 1-cm of spacing between the membrane and TCE solution, so the solution temperature might eventually reach the MIP temperature after a period of exposure. However, the solution temperature was not measured, so for data evaluation purposes, the solution temperature was assumed to be that of the MIP.

A series of experiments was completed with the membrane at 24, 50, 60, 70, and 100 °C to determine the mass of TCE extracted from the headspace of the 50 mg/L TCE solution. Figure 4.13 shows the average membrane separation factor for each of the headspace experiments. The membrane separation factor from 24 to 80°C has an average of 10.3, but then increases to 48 for the membrane at 100°C. The variability of the membrane separation factor had minimum values of +/- 6 and 7% for the membrane temperatures of 60 and 70°C respectively, and a maximum value of approximately +/- 30% for the membrane at 24, 50, and 100°C. The separation factor variability for the membrane at 100°C was the result of the heat pulses generated from the "on-off" heater block controller that occurred at approximately 4.2 and again at 6.6 minutes (Figure 4.12). The separation factor variability for the membrane at 24 and 50°C was due to the variation in water permeation through the membrane while the rate of TCE permeation remained consistent (data not shown) as in Figure 4.12. The fluctuation in water vapor migration through the membrane was potentially

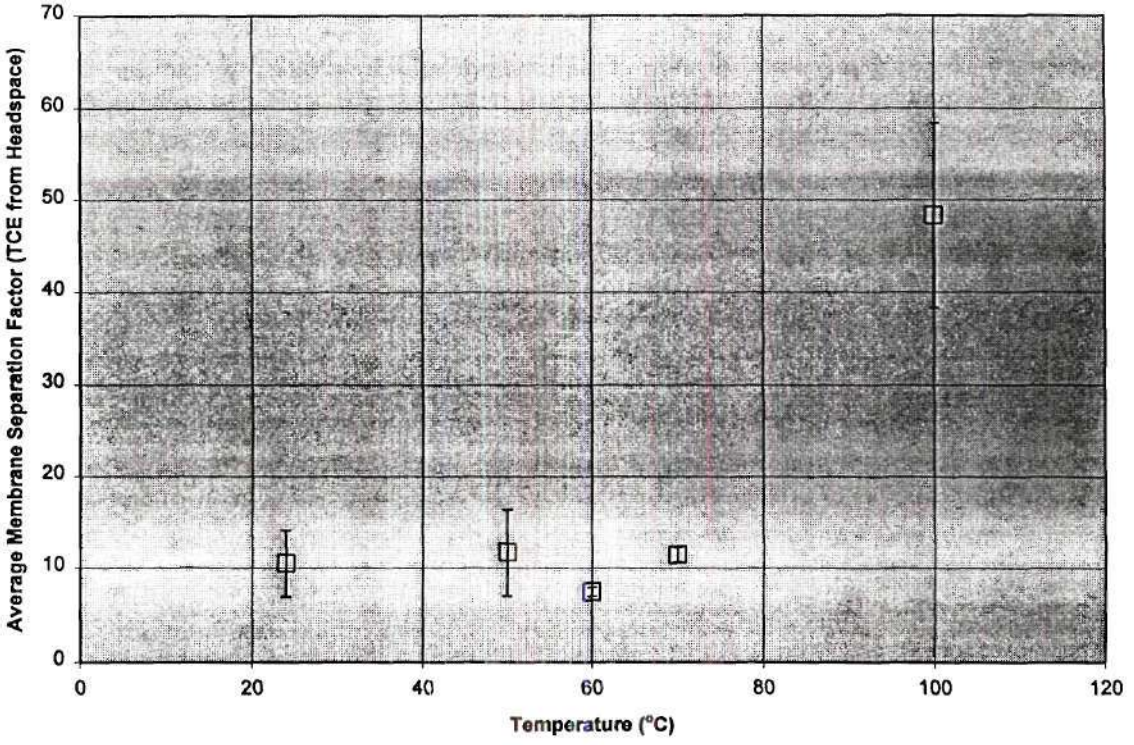

Figure 4.13 – Average membrane separation factor for TCE from the headspace of a 50mg/L solution as a function of temperature.

due to TCE vapor condensing within the pore spaces (capillary condensation), and reducing the amount of water migrating through the membrane (Baker, 2000).

Another series of experiments involved pumping a 50mg/L TCE solution through a small 2mL chamber attached to the membrane exterior. Figure 4.14 shows the results from one of the experiments completed with the MIP membrane operating at 40°C and the 2mL chamber filled with 20-30 Ottawa sand. Also plotted on Figure 4.14, is the overall pervaporation separation factor calculated for each analysis result using:

$$\beta_{pervap} = \frac{\text{Ion 132 Abundance / Ion 18 Abundance}}{K_H C_{TCE} / \text{density of } H_2O} \qquad (4.23)$$

This experiment was repeated with the membrane operating at 24, 40, 60, and 80°C. Figure 4.15 shows the average pervaporation separation factor for each of the experiments. The assumption that the aqueous phase temperature is the same as the stabilized MIP heater block temperature is reasonable since the aqueous phase in equilibrium with the membrane is directly in contact with the membrane.

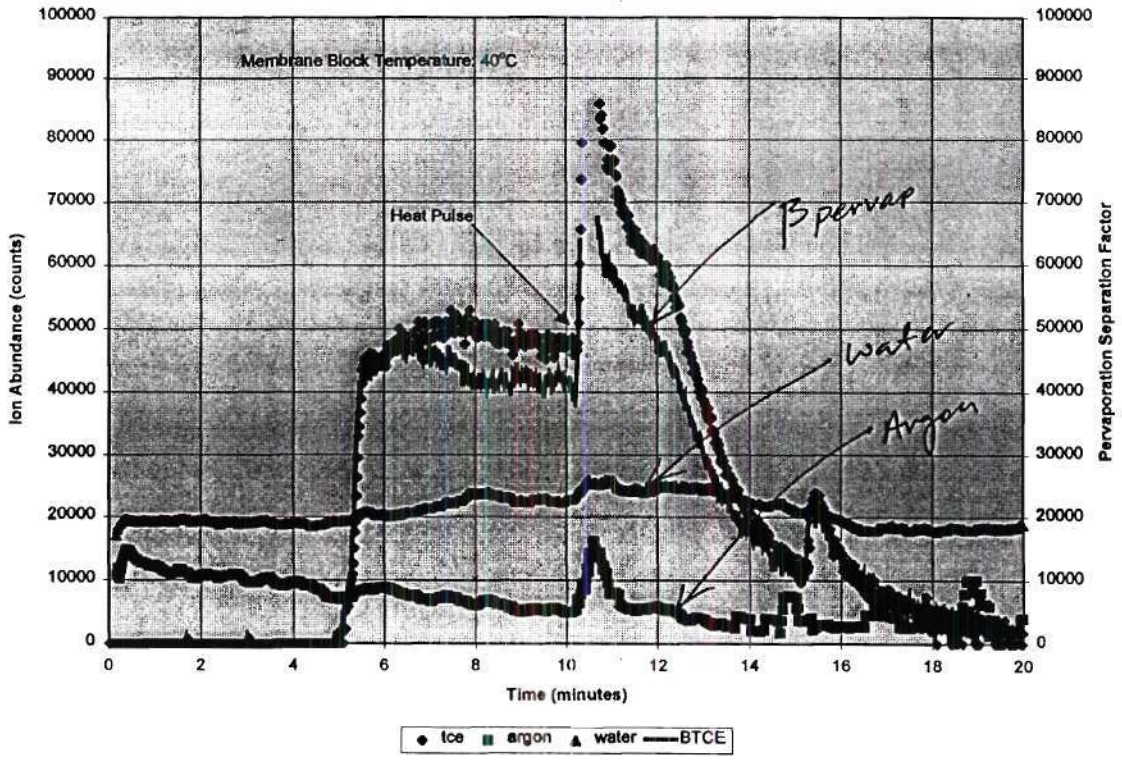

Figure 4.14 – Transfer of TCE from a 2mL volume filled with 20-30 mesh Ottawa sand and a 50 mg/L TCE solution into the MIP.

Figure 4.15 shows that the pervaporation factor was consistently near a value of approximately 50,000 once the membrane achieved a temperature of 40°C. The slight increase in average pervaporation factor that occurred when the membrane temperature was

increase to 80°C was accompanied by a large increase in pervaporation factor variance. The variability of the pervaporation separation factor had a minimum value of approximately +/- 6% for the membrane temperatures from 24 to 60°C, and a maximum value of approximately +/- 40% for the membrane at 80 and 120°C. The pervaporation factor variability for the membrane at 80°C was the result of the heat pulse generated from the "on-off" heater block controller that occurred at approximately 10 minutes (Figure 4.14).

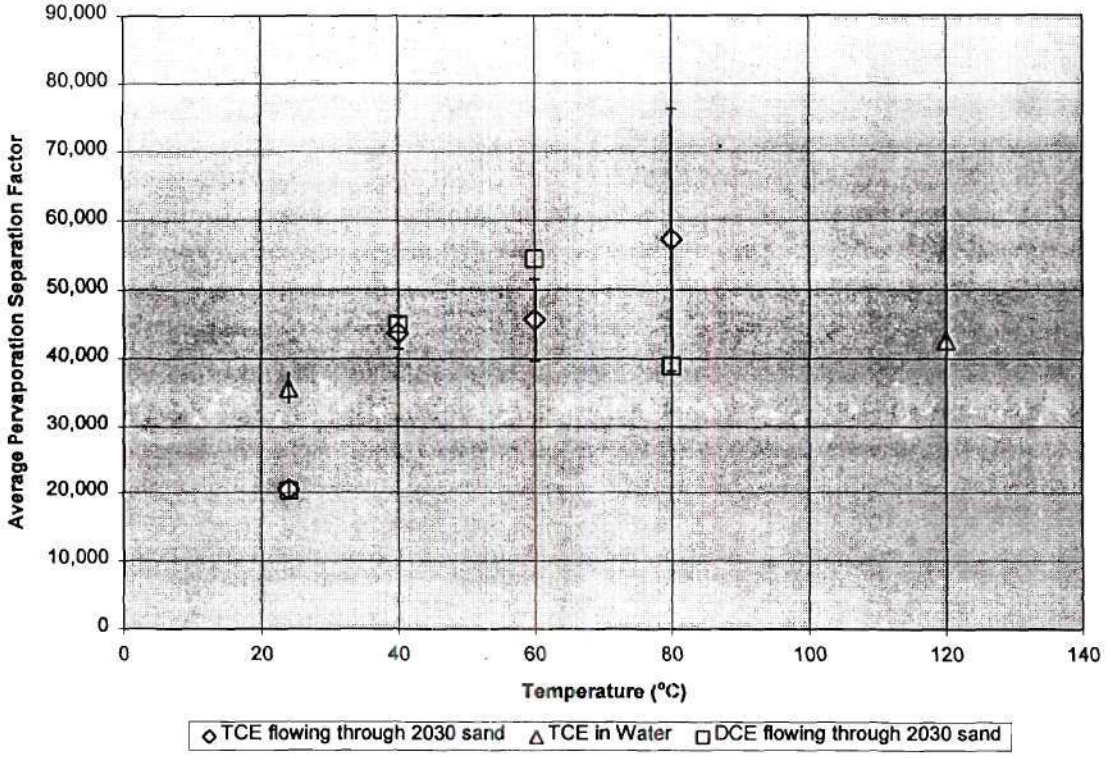

Figure 4.15 – Average pervaporation separation factor for a 50 mg/L TCE solution flowing past the laboratory-scale MIP membrane.

Baker (2000) reported pervaporation separation factors of near 40,000 for the separation of TCE from water by an ethylene-propylene copolymer membrane. However, for general industrial applications the typical separation factors for most VOCs are in the range of 200 to 1000.

One important feature missed by presenting the average separation factors (Figures 4.13 and 4.15) is the time required to reach peak separation. Figure 4.16 shows that in general, approximately 2.5 minutes were required to reach a peak pervaporation separation factor with the membrane at 24°C when exposed to gas phase or sand and water, while 20 minutes were required for water alone (data not shown). Approximately 1 minute was required to reach a peak pervaporation factor for membrane temperatures above 40°C. Increasing the membrane temperature above 40°C did not result in a significant decrease in the time required to reach peak recovery of TCE.

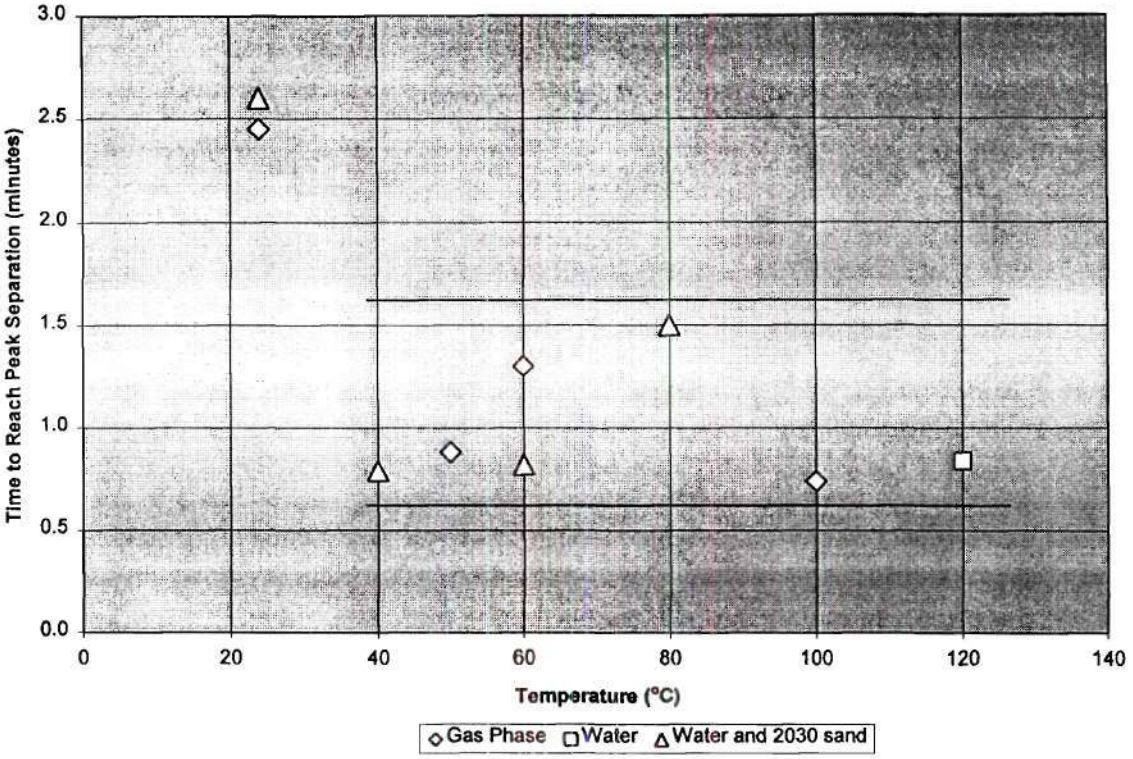

Figure 4.16 – Time to reach peak pervaporation separation factor with increasing membrane temperature.

4.2.4 In-Situ Mass Transfer Temperature Dependence

The dependence of recovering TCE from the subsurface for membrane temperatures of 60 and 120°C was evaluated during the completion of the second field test. Depth discrete samples were collected at comparable depths and approximately one meter apart. The first measurement was completed with the MIP heater block at 120°C and then a second, separate sampling effort was completed with the MIP heater block at 60°C. Figure 4.17 shows that there was no apparent differences in pervaporation separation factors between samples collected at 120°C and 60°C.

The baseline pervaporation factor for the samples collected at 60°C have values of approximately 10,000, while the baseline pervaporation factor values for samples collected at 120°C are zero. The difference is due to the lack of TCE ions in the sample collected at 120°C for the initial 73 seconds and then again after 170 seconds. There was also a difference in the amount of water ions present in the carrier gas between samples. The sample collected with the membrane at 120°C contained an average of approximately 12,500 water ions (counts) while the sample collected at 60°C contained an average of approximately 23,000 water ions (counts) (data not shown).

Based on this information, it is suggested that the aqueous phase was in contact with the membrane exterior for the sample collected with the membrane at 60°C, while the aqueous phase was not in contact with the membrane for the sample collected with the membrane at

120°C. Therefore, increasing the membrane temperature does cause the aqueous phase to move away from the membrane surface. This has been interpreted as necessary to facilitate the transfer of TCE from the subsurface into the MIP and to potentially minimize adsorption

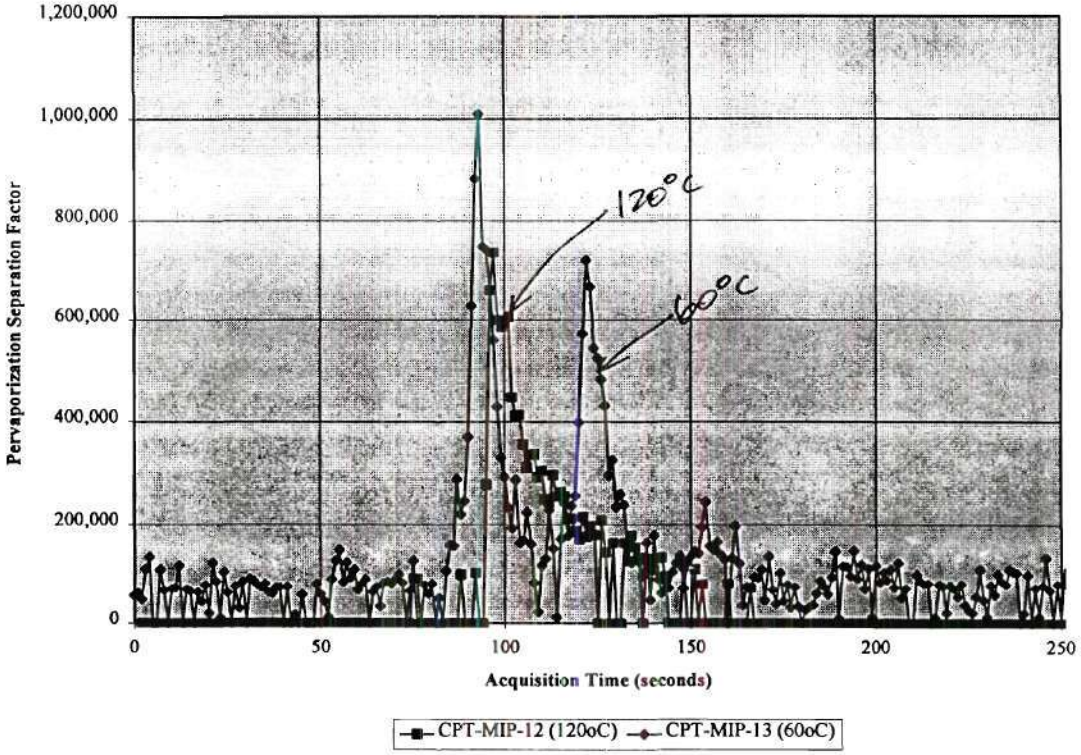

Figure 4.17 – Comparison of permeation separation factors for collocated samples collected at 65 feet bgs at the SRS, C Burning Pit Site.

of TCE onto the membrane between sample collection events (Nadolishny, 2001). However, both the laboratory and field data collected as part of this study show that TCE transfer is weakly temperature dependent once the membrane is above 40°C. Increasing membrane temperature leads to greater variance in the amount of TCE transferred per time and is the leading cause of the systematic bias observed in previous field efforts.

5.0 Conclusions

The results of the temperature profile experiments demonstrate that the internal MIP thermocouple temperature cannot be used to directly infer temperature external to the MIP. The difference between the temperature indicated by the thermocouple within the MIP heater block and that of the membrane exterior can be as great as 40°C. Soil thermal properties cannot be determined using the time rate of change of MIP temperature. Significant thermal influence does not extend beyond 1cm from the membrane as the result of MIP operation.

Gas flow through the MIP membrane can be described by Knudsen diffusion relationships, which show that differences in permeation rate between species is proportional to differences in the inverse of square roots of their molecular weights, also known as Graham's law. The

membrane within the laboratory-scale MIP is micro-porous with a mean pore diameter of from 122 to 400 angstroms. The portion of the membrane surface area available for gas transport ranges from 3.6 to 4.6%.

A theoretical prediction of TCE flux through the membrane from an aqueous solution containing 50 mg/L of TCE predicts at peak rate at 100°C which corresponds to the maximum Henry's coefficient.

Pervaporation was used to describe the separation of TCE from aqueous solutions. A separation factor for the membrane and overall process was used to evaluate TCE transfer from the gas and aqueous phases. The membrane separation factor for the laboratory-scale MIP membrane operating from 24 to 80°C has an average of 10.3, but increased to 48 for the MIP operating at 100°C. The variability of the membrane separation factor had a minimum value of approximately +/- 6% for the MIP operating at temperatures of 60 and 70°C respectively, and a maximum value of approximately +/- 30% for the MIP operating at 24, 50, and 100°C. The separation factor variability for the membrane at 100°C was the result of heat pulses generated from the "on-off" heater block controller. The separation factor variability for the MIP operating at 24 and 50°C was due to the variation in water permeation through the membrane while the rate of TCE permeation remained consistent. The fluctuation in water vapor migration through the membrane was potentially due to TCE vapor condensing within the pore spaces (capillary condensation), and reducing the amount of water migrating through the membrane (Baker, 2000).

The overall pervaporation separation factor was consistently near a value of approximately 50,000 once the membrane achieved a temperature of 40°C. A small increase (to approximately 57,000) in average pervaporation factor occured when the membrane temperature was increased to 80°C, but was accompanied by a large increase in pervaporation factor variance. The variability of the pervaporation separation factor had a minimum value of approximately +/- 6% for the MIP operating at temperatures from 24 to 60°C, and a maximum value of approximately +/- 40% for the MIP operating at 80 and 120°C. The pervaporation factor variability for the membrane at 80°C was the result of a heat pulse generated from the "on-off" heater block controller during sample collection.

In general, approximately 2.5 minutes were required to reach a peak pervaporation separation factor for the MIP operating at 24°C, while approximately 1 minute was required to reach a peak pervaporation factor for the MIP operating at temperatures above 40°C. Increasing the membrane temperature above 40°C did not result in a significant decrease in the time required to reach peak recovery of TCE.

In-situ field measurements show that there was no distinct difference between the amount of TCE recovered in depth discrete samples collected by the MIP operating at temperatures of 60 and 120°C. The presence of twice the number of water ions in the sample collected while operating the MIP at 60°C as compared to 120°C, showed that the aqueous phase was in contact with the membrane during collection of the 60°C sample. Achieving temperatures greater than the boiling point of TCE (86.7°C) or water (100°C) was not necessary to facilitate extraction of TCE from the subsurface into the MIP.

While raising the temperature of the MIP membrane is theoretically appealing (see Figure 4.11), the result of trying to maintain a MIP operating temperature of 120°C in the subsurface raises many conflicting forces. The laboratory and field work completed to date show that operating the existing MIP at higher temperatures may not yield significantly greater contaminant mass transfer. The work completed in this report suggests that the goal is to raise the membrane temperature to alleviate surface forces that cause the adsorption of solutes and can result in a significant time lag between membrane exposure and solute permeation.

The current method of providing power to the membrane heater block via the "on-off" temperature feedback control is the leading cause of the systematic bias observed in previous field efforts. It is recommended that the membrane be heated with a proportional power supply with the feedback temperature set-point between the limits of 40 and 80°C.

6.0 Literature Cited

Baker, R.W., Membrane Technology and Applications. McGraw-Hill, Hightstown, New Jersey, 2000

Environmental Security Technology Certification Program (ESTCP), Validation of the Site Characterization and Analysis Penetrometer System (SCAPS) Membrane Interface Probe System. http://www.estcp.com/projects/cleanup/, 2001

Costanza, J; Davis, W; Rapid Detection of Volatile Organic Compounds in the Subsurface by Membrane Introduction into a Direct Sampling Ion Trap Mass Spectrometer. Field Analytical Chemistry and Technology, Volume 4, Issue 5, November, 2000

Cunningham, R.E. and Williams, R.J.J, Diffusion in Gasses and Porous Media. Plenum Press, New York, 1980

Couvillion, R.J., Heat and Mass Transfer in a Semi-Infinite Moist Soil with a Drying Front Present. Ph.D. dissertation, Georgia Institute of Technology, Atlanta, Georgia, 1982

CRC Handbook of Chemistry and Physics, 82nd Edition ISBN: 0849304822 Cat. No.: 482 Published on: 6/8/2001

Choi, JG, Do, D.D., and Do, H.D., Surface Diffusion of Adsorption Molecules in Porous Media: Monolayer, Multilayer, and Capillary Condesation Regimes. Industrial Engineering Chemistry Research, 40, 4005-4031, 2001

Cussler, E.L., Diffusion, mass transfer in fluid systems. 2nd Edition, Cambridge University Press, 1997

Edwards A.L., Computer Heat-Conduction Calculations - a Compilation of Thermal Properties Data. UCRL-50589, 1969

Grigoriev, I.S., Meilikhov, E.Z., and Radzig, A.A., Handbook of Physical Quantities, CRC Press, Boca Raton, FL, 1997

Healy, J.J., de Groot, J.J., and Kestin, J., The theory of the transient hot-wire method for measuring thermal conductivity. Physica 82C: 392-408, 1976

Heron, G., Christensen, T.H., Enfield, C.G., Henry's Law Constant for Trichloroethylene between 10 and 95°C. *ES&T*, 32, 1433-1437, 1998

Philip, J.R. and De Vries, D.A., Moisture movement in porous materials under temperature gradients. Trans. Amer. Geophysical Union, 38(2): 222-231, 1957

Porter, P.C., Handbook of Industrial Membrane Technology. Noyes Publications, Park Ridge, New Jersey, 1990

Nadolishny, A., MIP Output Interpretation. nedatek incorporated, 2001

Shelby, J.E., Handbook of Gas Diffusion in Solids and Melts. ASM International, Materials Park, Ohio, 1996

Wise, M. B., Thompson, C. V., Merriweather, R., and Guerin, M., Review of Direct MS Analysis of Environmental Samples, Field Analytical Chemistry and Technology, 1(5):251-276, 1997